Rainfall estimates from opportunistic sensors in Germany across spatio-temporal scales

Maximilian Graf, Abbas El Hachem, Micha Eisele, Jochen Seidel, Christian Chwala, Harald Kunstmann, András Bárdossy

Angaben zur Veröffentlichung / Publication details:

Graf, Maximilian, Abbas El Hachem, Micha Eisele, Jochen Seidel, Christian Chwala, Harald Kunstmann, and András Bárdossy. 2021. "Rainfall estimates from opportunistic sensors in Germany across spatio-temporal scales." *Journal of Hydrology: Regional Studies* 37: 100883. https://doi.org/10.1016/j.ejrh.2021.100883.

Journal of Hydrology: Regional Studies 37 (2021) 100883

Contents lists available at ScienceDirect

Journal of Hydrology: Regional Studies

journal homepage: www.elsevier.com/locate/ejrh

Rainfall estimates from opportunistic sensors in Germany across spatio-temporal scales

Maximilian Graf [a,c,*], Abbas El Hachem [b], Micha Eisele [b], Jochen Seidel [b], Christian Chwala [a,c], Harald Kunstmann [a,c], András Bárdossy [b]

[a] Institute of Meteorology and Climate Research, Karlsruhe Institute of Technology, Campus Alpin, Garmisch-Partenkirchen, Germany
[b] Institute for Modelling Hydraulic and Environmental Systems, University of Stuttgart, Stuttgart, Germany
[c] Institute of Geography, University of Augsburg, Augsburg, Germany

ARTICLE INFO

Keywords:
Rainfall mapping
Opportunistic sensing
Personal weather stations
Commercial microwave links

ABSTRACT

Study region: The study region is Germany and two sub-regions in Germany, i.e. the state of Rhineland-Palatinate and the city of Reutlingen.

Study focus: Opportunistic rainfall sensors, namely personal weather stations and commercial microwave links, together with rain gauge data from the German Weather Service, were used in different combinations to derive rainfall maps with a geostatistical interpolation framework for Germany. This kriging type framework considered the uncertainty of opportunistic sensors and the line structure of commercial microwave links. The resulting rainfall maps were compared to two gauge-adjusted radar products and evaluated to three reference gauge datasets in the respective study regions on both daily and hourly basis.

New Hydrological Insights for the Region: The interpolated rainfall products from opportunistic sensors provided good agreement to the reference rain gauges. The dataset combinations including information from the opportunistic sensors performed best. The addition of rain gauges from the German Weather Service did not consistently lead to an improvement of the interpolated rainfall maps. On the country-wide, daily scale the interpolated rainfall maps performed well, but the gauge-adjusted radar products were closer to the reference. For the regional and local scale in Rhineland-Palatinate and Reutlingen with an hourly resolution, the interpolated rainfall maps outperformed the interpolated product from DWD rain gauges and showed a similar agreement to the reference as the radar products.

1. Introduction

Reliable rainfall measurement is crucial for monitoring and understanding the hydrologic cycle and climate variability. It delivers important information for water-resource management, agriculture, urban planning, as well as for weather, climate, and hydrological modelling. Several measurement devices for rainfall observations were developed in the past. While rain gauges of different types are used since the nineteenth century, weather radar observations are operated for the past decades. The spatial and temporal coverage of such measurement networks are unevenly distributed over the globe. Compared to other regions, the rain gauges and weather radars in Germany form a dense observation network (Lorenz and Kunstmann, 2012). Still, depending on the spatial and temporal scale of a

* Corresponding author.
E-mail address: maximilian.graf@kit.edu (M. Graf).

https://doi.org/10.1016/j.ejrh.2021.100883
Received 21 December 2020; Received in revised form 19 July 2021; Accepted 25 July 2021
Available online 7 August 2021

rainfall event, rainfall estimates can still be uncertain. For example, small convective events can be underestimated by weather radars or even missed completely by a network of rain gauges. The respective disadvantages of the individual measurement systems are the reason behind potentially uncertain estimates of the spatio-temporal distribution of rainfall (Cristiano et al., 2017). Quantitative precipitation estimates (QPE) from weather radars suffer from an uncertain Z–R relationship, beam blockage and ground clutter amongst others (Berne and Krajewski, 2013). Rain gauges can underestimate rainfall due to wind but more importantly the spatial and temporal variability of rainfall is not fully captured by point observations (Pollock et al., 2018).

New opportunities of measuring meteorological data are emerging with the increasing number and availability of opportunistic sensors in the last years (Zheng et al., 2018). Clark et al. (2018) used humidity, temperature and air pressure from personal weather stations (PWSs) to track the path of a hailstorm. The same variables from PWSs together with air pressure, temperature, and radiation from cell phones as well as rainfall estimates from commercial microwave links (CMLs) were used to examine a frontal system and the urban heat island effect over Amsterdam (de Vos et al., 2020).

Various different opportunistic rainfall sensors have already been investigated: the attenuation along satellite TV link path due to rainfall was exploited (Barthés and Mallet, 2013; Mercier et al., 2015). Windshield wiper frequency regulated by the optical rainfall sensor of a car were used to derive binary rainfall information (Mahoney and O'Sullivan, 2013; Rabiei et al., 2013). Rainfall estimates were derived from camera footage of rain (Allamano et al., 2015; Jiang et al., 2019). With the emerging 5G network and the growing number of devices connected to the Internet of Things, the number of potential sensors will further increase (Balsamo et al., 2018; McCabe et al., 2017; Tauro et al., 2018). In this study we use rainfall data from PWSs and commercial microwave links (CMLs).

The nearly linear relationship between rainfall and the attenuation of microwave link signals operating with frequencies between 10 and 40 GHz is known for several decades (Atlas and Ulbrich, 1977). With the growth of modern telecommunication infrastructure, for which CMLs provide a large portion of the backhaul network, an increasing number of microwave links became available and CMLs were introduced as opportunistic rainfall sensor almost 15 years ago (Messer et al., 2006; Leijnse et al., 2007). Deriving rainfall estimates from CMLs can be challenging because of several issues. Erratic signal behavior due to refraction, reflection, or multipath propagation as well as unknown relation to meteorologic variables cause fluctuation of the signal (Upton et al., 2005; van Leth et al., 2018). Likewise, wet CML antennas can cause additional attenuation during and also after rainfall events until they are dry again (Fencl et al., 2019). Rainfall estimates from CMLs were derived for diverse regions in the world mainly in Europe (e.g. Andersson et al., 2017; Fencl et al., 2017; Overeem et al., 2016b; Roversi et al., 2020; van de Beek et al., 2020), but also for other countries as for example Israel (Ostrometzky and Messer, 2018), Brasil (Rios Gaona et al., 2018), West Africa (Doumounia et al., 2014) and, China (Song et al., 2020). An overview of the background and challenges in rainfall estimation from CMLs was given by Chwala and Kunstmann (2019) and Uijlenhoet et al. (2018), respectively. Rainfall maps were derived from CMLs, often neglecting the path-integrated nature of the estimated rain rate but rather using the center of each CML as a theoretical point measurement (Graf et al., 2020; Overeem et al., 2016b). Some dedicated mapping algorithms were introduced but not analyzed on a larger scale (Liberman et al., 2014; Beek et al., 2020; Haese et al., 2017)

The potential and challenges using rainfall data from PWSs were first shown by de Vos et al. (2017). PWSs also provide other meteorological information (Bell et al., 2013; Jenkins, 2014), but for our study, from here on, PWSs will only refer to personal weather stations measuring rainfall. PWSs are rain gauges which are set up by individual citizens. Data from PWSs are prone to numerous error sources ranging from calibration issues to poor maintenance and unfavourable positioning. Therefore, a thorough quality check of PWSs data is necessary. An intrinsic approach using information of neighboring PWSs was tested in the Netherlands (de Vos et al., 2019). The Norwegian Meteorological Institute deployed an automatic data quality control for their meteorological station data which is supplemented by opportunistic data e.g. for temperature (Båserud et al., 2020). Another approach presented by Bárdossy et al. (2021) used data from a trustworthy primary network and a geostatistical method combined with rank statistics. This approach is also used in our study to remove and bias correct suspicious PWSs and CML data with modifications of the filtering approach to account for the line characteristic of the CML data.

This study aims to provide (1) a large scale evaluation of rainfall estimates from two types of opportunistic rainfall sensors, (2) a geostatistical interpolation framework and (3) a related performance analysis of the derived rainfall maps using data from opportunistic sensors, official rain gauges and various combinations of these datasets. The performance analysis is carried out on different spatial and temporal scales. The interpolation framework takes the specific characteristics and uncertainties of the sensors into account and combines rainfall information from point and line sources with individual weights. These sensors are official rain gauges from the German Meteorological Service (DWD), PWSs data obtained from Netatmo, and CML data obtained from Ericsson, in Germany. The question we raise is, how accurate can opportunistic sensors measure rainfall on a country wide, regional, and local scale? Specifically: in Germany, the federal state of Rhineland-Palatinate, and the city of Reutlingen, respectively?

2. Study region and data

2.1. Study region

The study region is Germany and our analysis was carried out on a national scale for the whole of Germany with 357,386 km^2, on a regional scale for the state of Rhineland-Palatinate with 19,847 km^2 and on a local scale for the city of Reutlingen with 87 km^2. Rainfall in Germany is falling year-round with a peak during the summer months. The driest regions are located in the northeast with mean rainfall amounts of 450 mma^{-1} year. Highest rainfall amounts occur in the Central German Uplands with over 1000 mma^{-1} and in the Alps with up to 2000 mma^{-1}. Rainfall in the northern part of Germany is mostly influenced by synoptic driven processes while convective events become more frequent southwards. Rhineland-Palatinate is situated in the mid-west of Germany with yearly rainfall

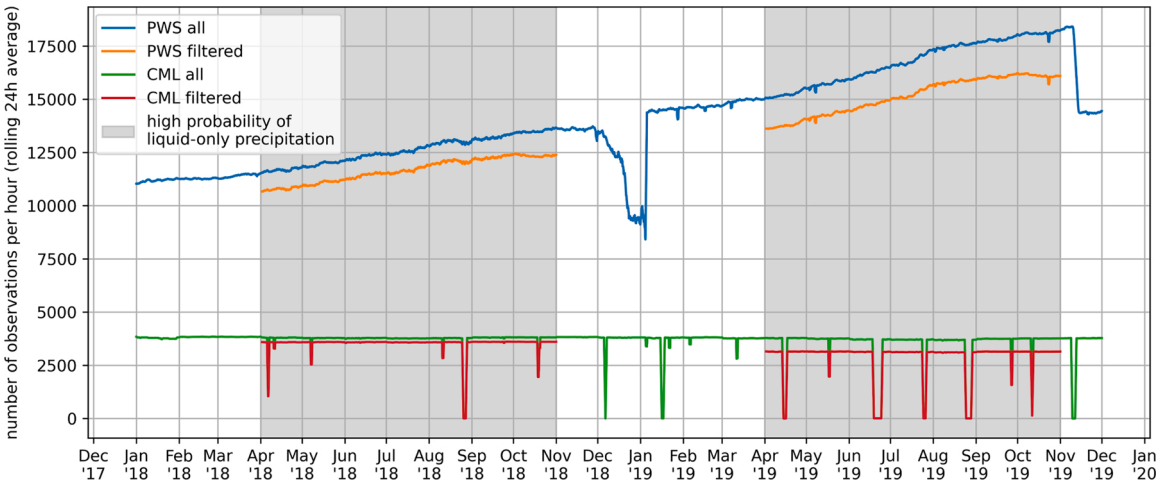

Fig. 1. Availability of PWS and CML data for the years 2018 and 2019 before and after the processing and filtering.

amounts between 500 and 800 *mm* between the Rhine Valley and the low mountain ranges of Taunus and Hunsrück. The city of Reutlingen is located in the south-western state of Baden-Wuerttemberg approximately 30 *km* south of the state capital Stuttgart.

The density of hydro-meteorologic measurements over Germany, and therefore also for Rhineland-Palatinate and Reutlingen, is high compared to most other parts of the world (Lorenz and Kunstmann, 2012). The German Weather Service (DWD) operates a weather radar network and roughly 2000 rain gauges with daily and hourly temporal resolution. Several state agencies and private companies additionally operate hundreds of rain gauges, which are partly used in rainfall products of the DWD. The continuous measurement of precipitation in Germany started more than a hundred of years ago with many gauge locations being sampled for multiple decades (Hellmann, 1907). Therefore, the measurement of precipitation with additional opportunistic sensors and the generation of interpolated products from these sensors would not seem to be of primary importance in Germany.

Yet, the spatio-temporal variability of rainfall cannot be captured completely with common products derived from rain gauges and weather radars. This is especially the case for short duration and high intensity rainfall which can cause flash floods (Berne et al., 2004; Emmanuel et al., 2012; Ochoa-Rodriguez et al., 2015). A striking example is the devastating flash flood in the city of Braunsbach in 2016. In a 10 *km* radius around Braunsbach, only one rain gauge with a daily resolution is located. Radar data underestimated the rainfall measured from the rain gauge by 30 percent, therefore it is uncertain whether the radar measurements of the peak rainfall several kilometers away from the gauge was estimated correctly (Bronstert et al., 2018). With the increasing density of opportunistic sensor networks, like the ones used in this study, the probability that such sensors detect small scale events and their variability is also increasing. We use the opportunity of having several independent rain gauge networks in Germany to evaluate the rainfall maps derived from opportunistic rainfall sensors with our mapping approach on three different scales: On the country-wide scale for the whole of Germany, on the regional scale for Rhineland-Palatinate and on the local scale for Reutlingen. We expect the higher network density of the opportunistic sensors to be beneficial especially on the regional and local scale.

2.2. Opportunistic rainfall data

We use two types of opportunistic rainfall data, namely PWS data from the Netatmo network (https://weathermap.netatmo.com) and CML data from Ericsson. Netatmo is a company selling PWSs among other smart-home devices. Their basic PWS system (which provides measurements of temperature, humidity, air pressure) can be extended with an unheated tipping bucket gauge for rainfall measurement. These rain gauges have a collecting area of 125 cm^2 and a temporal resolution of five minutes. de Vos et al. (2019) gives further technical details to Netatmo PWSs. If the owner agrees, data from the PWSs is uploaded to Netatmo's weather map. Data is then available via an API in temporal resolutions down to five minutes. The used dataset consists of all freely available PWSs data from Netatmo in Germany in 2018 and 2019. Fig. 1 shows their continuously growing number of up to 15,000 by the end of our study period. The reason for the decreasing numbers during winter was not investigated. A possible explanation could be battery failure due to cold temperatures. The spatial distribution of PWSs in Germany follows roughly the population density with most PWSs situated in urban areas as for example shown in the map in Fig. 4.

CML data are typically not publicly available but need to be provided by telecommunication providers. We receive data from 3904 CMLs from Ericsson in Germany via a near-real time data acquisition system (Chwala et al., 2016). The CML lengths range from 0.3 to 30 *km* and their frequencies from 10 to 40 *GHz*. The spatial distribution of CMLs is highly unbalanced throughout Germany. We currently only have access to a subset of CMLs which is only a small part of the more than 100,000 CMLs installed in Germany (Bundesnetzagentur, 2017). The distribution of the CMLs in this subset is not representative for the general distribution of CMLs in Germany. More information on the characteristics of this CML dataset are available from Graf et al. (2020).

The analyzed periods are the summer season from April to October 2018 and 2019 as shown in Fig. 1. For previous years, the

Table 1
Overview of used datasets: (a) input data for the interpolation framework, (b) radar datasets used for comparison, and (c) reference rain gauge datasets used for the evaluation.

Name	Number of sensors	Resolution	Operator
a) Rain gauge and opportunistic data used in the interpolation framework			
DWD_{auto}	968	hourly	DWD
(filtered) PWSs	10,500 – 16,200	hourly	private/Netatmo
(filtered) CMLs	3150 – 3600	hourly	Ericsson
b) Radar datasets used for comparison			
RADOLAN-RW	900 × 900 grid	hourly	DWD
RADKLIM-YW	1,100 × 900 grid	hourly	DWD
c) Reference gauge datasets			
DWD_{man}	1062	daily	DWD
RLP	169	hourly	State Agrometeorological Agency Rhineland-Palatinate
RT	10	hourly	City of Reutlingen

availability of PWSs was significantly lower and our country-wide data acquisition for CMLs in Germany started in August 2017. We excluded months with high probability of snow, since performance for both sensors decreases in winter. PWSs are not heated and CML suffer from snow and ice on their antennas as well as from large uncertainties of the relation between attenuation and snow and melting snow. Melting sown for example causes a many times higher attenuation than rain resulting in large overestimation of the precipitation event. An overview of all used datasets and their respective usage is given in Table 1.

2.3. Gauge and radar data

We use two different gauge datasets operated by the DWD. The first gauge dataset consists of 968 automatic pluviometers. We use the hourly and quality checked data from these rain gauges (referred to as DWD_{auto} from here onwards) in the interpolation framework (Section 3.3). The second gauge dataset (referred to as DWD_{man}) consists of 1062 manual rain gauges with a daily resolution. The collection diameter is 200 cm^2 and the gauges are heated. This dataset is used as a reference for the country-wide evaluation as it is independent of the DWD_{auto} data. Both DWD gauge datasets have a density of roughly one gauge per 300 km^2. A network of 169 hourly rain gauges in Rhineland-Palatinate is used for the evaluation on a higher temporal resolution. These gauges are operated by the State Agrometeorological Agency of Rhineland-Palatinate. This dataset has a spatial density of roughly one gauge per 100 km^2. For the evaluation on the local scale we use hourly data from ten rain gauges situated in the city of Reutlingen. The OTT pluviometers form a dense network of one gauge per 9 km^2.

We use two radar datasets in this study, namely, RADOLAN-RW and RADKLIM-YW provided by the DWD. RADOLAN-RW is a near-real time product with an hourly resolution. It is updated with 30 minutes lag time. The gridded dataset covers Germany with 900 by 900 grid cells with a 1 km resolution. It is a composite of 17 weather radars adjusted via a weighted combination of additive and multiplicative corrections from the DWD_{auto} gauge network (Bartels et al., 2004; Winterrath et al., 2012). RADKLIM-YW is based on the same radar and gauge data as RADOLAN-RW but undergoes climatological adjustments, accounting for e.g. range-dependent underestimation and radar spokes due to beam blockage (Winterrath et al., 2018). The adjustments are carried out with hourly data (RADKLIM-RW), but are also applied to the 5-minute data (RADKLIM-YW) which we use here. The performance of radar and rain gauge products from the DWD were already analysed. While especially during winter and in small catchments the differences in daily, areal rainfall could exceed 50% (Kneis and Heistermann, 2009; Meissner et al., 2012), the mean yearly rainfall sums of DWD rain gauges and radar products compare well (Kreklow et al., 2019).

3. Methods

3.1. CML and PWS data preparation and processing

CML data cannot be converted to a rainfall estimate directly. Several processing steps are required to obtain rain rates from raw CML attenuation data. We use the processing routine described in Graf et al. (2020) with the exception of the classification of wet and dry periods where we use an improved method presented by Polz et al. (2020): First, CMLs with erratic data (e.g. from drifts, jumps or high levels of noise) are removed from the dataset using two filters based on monthly statistics of the CML raw data. Data gaps shorter than 5 minutes are interpolated linearly. Then, wet and dry periods are classified by a convolutional neural network trained to that specific task. For each identified rain event the baseline of the signal is derived from the precedent dry period. Using this event-specific baseline, attenuation values are calculated which are then corrected for the additional attenuation caused by raindrops on the CML antennas. From the final rain-induced attenuation the rain rate can be calculated using the $k - R$ relation, where k is the specific path attenuation (in $dBkm^{-1}$) and R is the rain rate (in mmh^{-1}). A detailed description of these steps as well as a large scale analysis can be found in Graf et al. (2020). We chose the new classification of wet and dry periods from Polz et al. (2020) because it reduces the false-positive rate (FPR) while keeping the false-negative rate (FNR) constant which is shown along with an evaluation of the combination of both methods for one month for the whole of Germany in Fig. 9 of Polz et al. (2020). All introduced CML processing

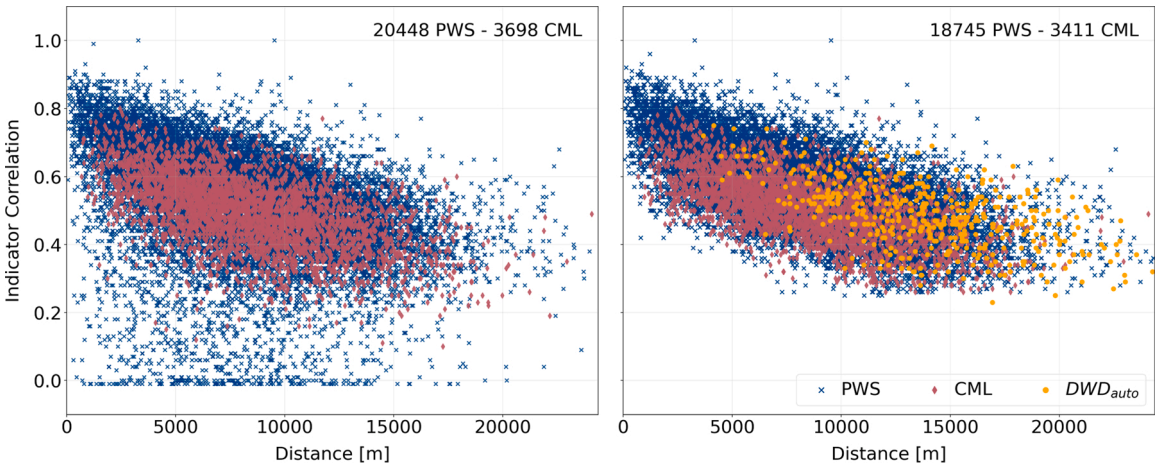

Fig. 2. Indicator correlations for 1h temporal resolution and a quantiles level of 0.99 between the PWS and CML networks and the nearest DWD_{auto} (the reference network in this case) stations before (left) and after (right) applying the filter for the year 2019. (For interpretation of the references to color in this figure legend, the reader is referred to the web version of this article.) The orange dots refer to the indicator correlation between the DWD_{auto} network stations.

routines can be found in the software package pycomlink (2021). The resulting data consists of rain rates averaged along the CMLs path with one minute temporal resolution. This data is then aggregated to an hourly resolution except for hours with gaps longer than 5 minutes which were not interpolated in the first step.

The reason for the five-minute interpolation, besides rare connection problems of the data acquisition system, is the engineering requirements of the CML network. For each CML the combination of a given path length with a microwave frequency is chosen so that, on average, the path attenuation due to heavy rain leads to a complete signal loss at the receiver only for some minutes per year. Because the choice of the frequency and the path length are constrained - only certain frequency bands are available, high frequencies are desired to allow more bandwidth, and path length is determined by the locations of CML towers - the maximum rain rate before signal loss is different for all CMLs. It can be as low as 40 mmh^{-1} but also above 150 mmh^{-1} e.g. for very short CMLs (1 km or shorter) or for short CMLs ($< 5\,km$) with low frequencies ($< 20\,GHz$). Therefore, for heavy rainfalls some CMLs do not provide accurate rainfall information.

The PWS data have been acquired via the Netatmo API in time steps of variable length of typically 5 minutes and aggregated to hourly resolution. Additional information regarding the Netatmo data acquisition can be found in de Vos et al. (2020). Compared to the hourly data of the Netatmo API, which accepts up to eleven missing five-minute values, we have removed all hours with more than one missing five minute value.

3.2. *Indicator correlation filter, event based filter and bias correction*

The filtering and bias correction approach introduced by Bárdossy et al. (2021) was the basis for filtering and bias correcting the PWS data in this study. The CML data was also treated with this approach even though they already were pre-processed with pycomlink which removed the worst performing CMLs from the dataset. Problems we still encountered in the CML derived rain rates were strong overestimation of melting snow (evident in April and October) and other false positive events caused by attenuation which was not induced by rain which the rather liberal filtering of pycomlink did not remove.

The main assumption behind the indicator correlation filter is that the specific PWS or CML values might be wrong but their ranks are correct, especially for the most intense events. Using a reference network such as the DWD_{auto} rain gauges, which are installed according to the WMO guidelines, the dependence between the nearest neighboring stations is investigated. For each location, the correlation value of the indicator series between the pairs of DWD_{auto}-PWS or DWD_{auto}-CML is compared to the values between the DWD_{auto} stations for similar separation distances and time periods. Hereby, information on how precipitation varies in space is acquired and PWS or CML locations with unreliable observations for high precipitation intensities are identified. For the CML data we used an extended version of the indicator correlation filter to account for the geometric line structure of the CMLs which is described in Appendix B while the basic principle of the filter was unchanged. The indicator correlation filter is applied on a yearly basis for all hourly PWS and CML data. Fig. 2 shows the results for the year 2019. After applying the filter, around 92% of the PWSs and of the CMLs remained. The number of PWSs in Fig. 2 refers to the overall number of PWSs providing data during 2019 while Fig. 1 shows the availability of PWS measurements at each point in time which causes the different values.

Even though the order of the values is assumed to be correct, the PWS and CML values remaining after the indicator correlation filter might have an unknown bias. The bias varies individually for each location and each observation. Therefore, the real precipitation amounts need to be estimated. This is done for the observed hourly data. For this purpose, the precipitation distribution functions of the DWD_{auto} stations are used. For a target location and a given time step, using the observed quantiles (PWS or CML), the

corresponding DWD_{auto} quantiles are derived and the corresponding precipitation amount is interpolated. Through this procedure the possible bias available at the PWS and CML locations is reduced. The resulting time series are used further on in this study. A more detailed description of both the indicator correlation filter and bias correction for the CML data can be found in Appendix B.

While the indicator correlation filter removes opportunistic sensors for a whole year some remaining sensors can suffer from erratic measurements for individual events. Possible reasons can be low battery or clogged funnels for PWSs as well as outages in the data acquisition or attenuation induced by other sources than rain for CMLs. We applied an event based filter after the bias correction which uses the variogram of the next 30 DWD_{auto} stations to cross-validate each sensor in order to remove faulty values. If a sensors' rainfall value differs too much from the value estimated by the variogram of the 30 stations (here three times the kriging standard deviation) it was rejected. In order to preserve higher rainfall values and to focus more on discarding false zeros, this filter used the square root of the rainfall sum. This was the only modification of the event based filter which first was shown in Bárdossy et al. (2021). Overall, this filter removed around 0.6% of the PWS data and 1.5% of the CML data.

3.3. Geostatistical interpolation framework

We developed a geostatistical interpolation framework which allows a combination of different data sources and their specific features and geometric properties. Let $\{x_1, \ldots, x_n\}$ be the locations of the DWD_{auto} observation points, $\{y_1, \ldots, y_m\}$ the locations of the PWSs (after filtering) and $\{L_1, \ldots, L_k\}$ be the line segments of the CMLs (after filtering). The estimation of the precipitation amounts Z at a given location $x*$ is done by a combined kriging approach in which both the increased uncertainty of the PWS and CML based precipitation is taken into account, and the CML's line structure is considered by using a block kriging type approach. The estimation is obtained in the form

$$Z(x^*) = \sum_{i=1}^{n} \lambda_i Z(x_i) + \sum_{i=1}^{m} \alpha_i Z(y_i) + \sum_{i=1}^{k} \beta_i Z(L_i) \tag{1}$$

With the additional condition of unbiasedness

$$\sum_{i=1}^{n} \lambda_i + \sum_{i=1}^{m} \alpha_i + \sum_{i=1}^{k} \beta_i = 1 \tag{2}$$

The weights $\mathrm{w}^T = (\lambda_1, \ldots, \lambda_n, \alpha_1, \ldots, \alpha_m, \beta_1, \ldots, \beta_k, \mu)$ can be obtained by solving the linear equation system

$$\mathrm{Aw} = \mathrm{c} \tag{3}$$

μ is the Lagrange multiplier introduced to ensure the fulfilment of the unbiasedness condition Eq. (2).
The matrix A is

$$\mathrm{A} = \begin{pmatrix}
\gamma(x_1,x_1) & \ldots & \gamma(x_1,x_n) & \gamma(x_1,y_1) & \ldots & \gamma(x_1,y_m) & \overline{\gamma}(x_1,L_1) & \ldots & \overline{\gamma}(x_1,L_k) & 1 \\
\vdots & \ddots & \vdots & \vdots & \ddots & \vdots & \vdots & \ddots & \vdots & \vdots \\
\gamma(x_n,x_1) & \ldots & \gamma(x_n,x_n) & \gamma(x_n,y_1) & \ldots & \gamma(x_n,y_m) & \overline{\gamma}(x_n,L_1) & \ldots & \overline{\gamma}(x_n,L_k) & 1 \\
\gamma(y_1,x_1) & \ldots & \gamma(y_1,x_n) & \gamma(y_1,y_1)+\varepsilon_y & \ldots & \gamma(y_1,y_m) & \overline{\gamma}(y_1,L_1) & \ldots & \overline{\gamma}(y_1,L_k) & 1 \\
\vdots & \ddots & \vdots & \vdots & \ddots & \vdots & \vdots & \ddots & \vdots & \vdots \\
\gamma(y_m,x_1) & \ldots & \gamma(y_m,x_n) & \gamma(y_m,y_1) & \ldots & \gamma(y_m,y_m)+\varepsilon_y & \overline{\gamma}(y_m,L_1) & \ldots & \overline{\gamma}(y_m,L_k) & 1 \\
\overline{\gamma}(L_1,x_1) & \ldots & \overline{\gamma}(L_1,x_n) & \overline{\gamma}(L_1,y_1) & \ldots & \overline{\gamma}(L_1,y_m) & \overline{\gamma}(L_1,L_1)+\varepsilon_L & \ldots & \overline{\gamma}(L_1,L_k) & 1 \\
\vdots & \ddots & \vdots & \vdots & \ddots & \vdots & \vdots & \ddots & \vdots & \vdots \\
\overline{\gamma}(L_k,x_1) & \ldots & \overline{\gamma}(L_k,x_n) & \overline{\gamma}(L_k,y_1) & \ldots & \overline{\gamma}(L_k,y_m) & \overline{\gamma}(L_k,L_1) & \ldots & \overline{\gamma}(L_k,L_k)+\varepsilon_L & 1 \\
1 & \ldots & 1 & 1 & \ldots & 1 & 1 & \ldots & 1 & 0
\end{pmatrix} \tag{4}$$

and the right hand side of the equation is

$$\mathrm{c}^T = (\gamma(x^*,x_1), \ldots, \gamma(x^*,x_n), \gamma(x^*,y_1), \ldots, \gamma(x^*,y_m), \overline{\gamma}(x^*,L_1), \ldots, \overline{\gamma}(x^*,L_k), 1) \tag{5}$$

Here for any pair of points, $\gamma(x_i, y_j)$ is the variogram value corresponding to the vector $x_i - y_j$. The combination of a point and a line segment requires a mean variogram value over the segment

$$\overline{\gamma}(x_i, L_j) = \frac{1}{|L_j|} \int_{L_j} \gamma(x_i, u) \ \mathrm{du} \tag{6}$$

and for the consideration of pairs of line segments L_i and L_j one has to calculate the corresponding mean value:

$$\overline{\gamma}(L_i, L_j) = \frac{1}{|L_i||L_j|} \int_{L_i} \int_{L_j} \gamma(u, v) \ \mathrm{du} \ \mathrm{dv} \tag{7}$$

The ε_y and the ε_L values in the diagonal of the matrix represent the uncertainty of measurements of the PWSs and the CMLs respectively. In our approach we selected a 10 % error. Experimental variograms were calculated for each one hour time step using the DWD_{auto} only and the filtered bias corrected PWS data only. The variograms were subsequently normalized, and a k-means clustering

Table 2
Interpolated rainfall products and their input data.

Abbreviation	Input data
DWD_{int}	DWD_{auto}
PWS_{int}	PWS
CML_{int}	CML
DWD_CML_{int}	DWD_{auto}, CML
DWD_PWS_{int}	DWD_{auto}, PWS
PWS_CML_{int}	PWS, CML
$DWD\_PWS\_CML_{int}$	DWD_{auto}, PWS, CML

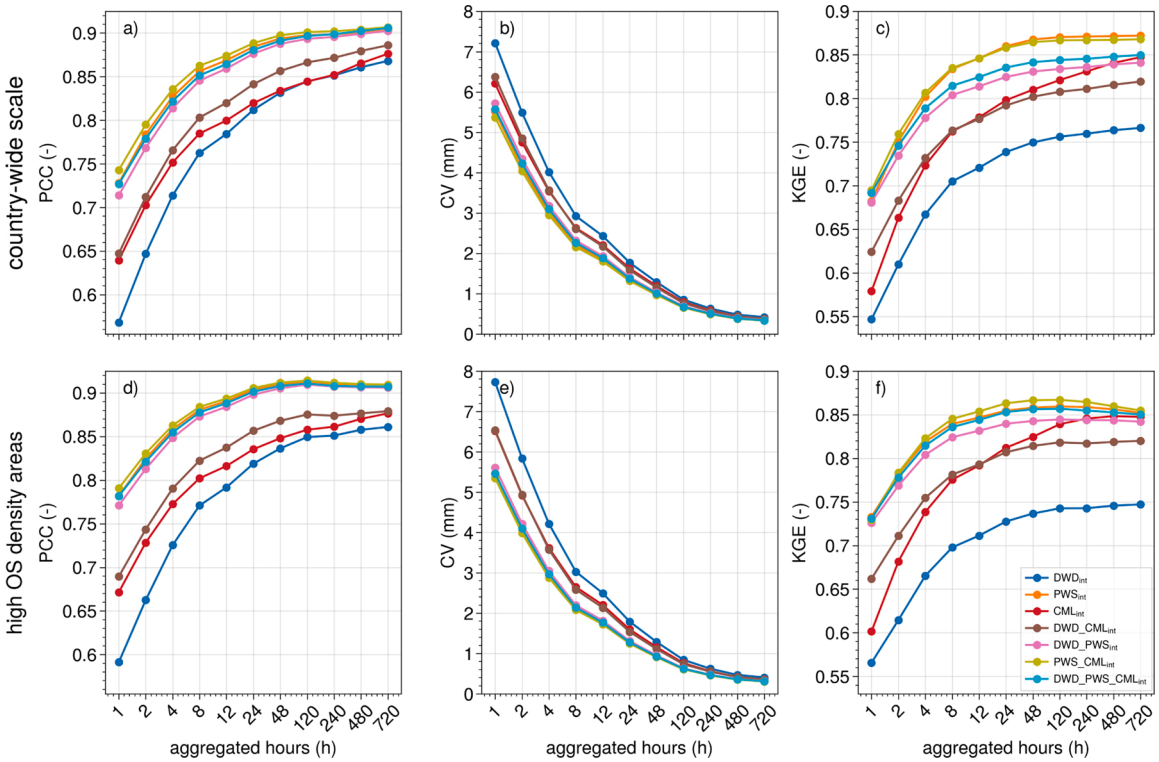

Fig. 3. Performance measures of the cross validation from the interpolation framework for different temporal aggregations. (a) to (c) show PCC, CV and KGE for all country-wide DWD_{auto} validation stations and (d) to (f) show PCC, CV and KGE for validation stations with more than 80 PWSs or CMLs in 20 *km* vicinity which have data available for the whole analysed period. Those are the 10 percent of the validation stations which are surrounded by the most opportunistic sensors.

algorithm was used to divide them into 4 different groups. Theoretical variograms were fitted to each center of the cluster. The fitted variograms differed mainly in the range which was between 12.5 and 40.0 *km*. The variograms based on the DWD_{auto} data showed no nugget effect, while the PWS based variograms had a nugget of about 10 %. This was the reason why the ε was selected as 10 % of the sill. The consideration of the length and orientation of the line segments is fully respected in this equation. If one would replace each line segment with its central point (as done e.g. in Overeem et al. (2016a)) the weights would be significantly different (see Fig. A1 for an example). All combinations of datasets and the respective interpolated products are given in Table 2.

4. Results and Discussion

4.1. Cross validation of the interpolated rainfall products

A leave one out cross validation is used to compare the performance between the interpolated products among each other at the location of the DWD_{auto} stations for temporal aggregations between one hour and 30 days. For the cross validation the target stations were removed for the whole procedure, the filtering, the assessment of the distribution function and for the interpolation of the precipitation amounts. This allows us to evaluate the performance of the different interpolation products at the location of each DWD_{auto} independently. As diagnostic measures, the Pearson's correlation coefficient (PCC), the coefficient of variation (CV) and the Kling-Gupta efficiency (KGE) as well as the false positive (FPR) and false negative rate (FPR) are used. Their definitions can be found in

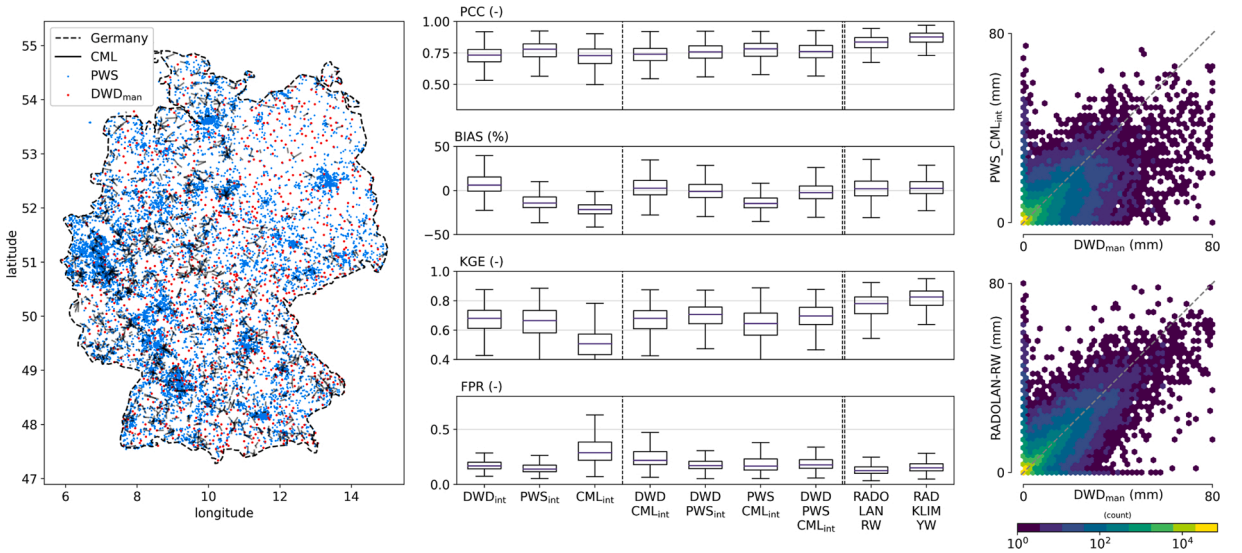

Fig. 4. Map of Germany with DWD_{man} gauges (reference), PWS locations and CML paths, boxplots of performance measures for the seven interpolated products as well as RADOLAN-RW and RADKLIM-YW against the reference. The vertical dashed line separates the interpolated products which are based on a single data set from the combined products and the double dashed line separates the radar products. On the right, scatter density plots of daily PWS-CML and RADOLAN-RW rainfall sums are compared to the reference.

Appendix C. Because DWD_{auto} was also used in four of the seven interpolation products, the validation was carried out as a leave-one-out cross validation. The results are shown in Fig. 3 (a) to (c) for all DWD_{auto} stations as validation stations and in (d) to (f) for a selection of ten percent of DWD_{auto} stations defined by the density of opportunistic sensors in close vicinity which we call selected validation stations from here on.

Two groups of interpolation products are visible for all measures and both selections of stations. This distinction was larger for the selected validation stations. One group contained PWS_{int} and the other combinations with PWSs, whereas the other group contained DWD_{int}, CML_{int} and their combination. PWS_{int} and the other combinations with PWSs performed better for all three performance measures. The interpolated products with opportunistic sensors had higher performance measures for the selected validation stations. DWD_{int} showed the worst performance for both all and selected validation stations. The performance of opportunistic sensors increased when only validations stations surrounded by many PWSs and CMLs were considered. We think that the heterogeneous distribution of opportunistic sensor networks of CMLs and PWSs shown in the map in Fig. 4 is the reason for this better performance. DWD_{auto} with its more homogeneous distribution performed similar between both validation station sets.

With increasing temporal aggregation the performance of all interpolated products increased. The difference between all and selected validation stations was highest at short aggregations of one to 12 hours for PCC and KGE. For the aggregations over days, they were similar. This emphasizes the influence of quality and amount of sampling points when interpolating rainfall on sub-daily temporal scales.

Overall, the combinations with PWSs had the highest performance values while the interpolation product which used all three possible datasets (DWD_PWS_CML_{int}) was not the overall best performing one, even though it contained the highest number of sampling points. A potential explanation is that DWD_{int} measurements are considered more reliable and hence have a higher weight in the block kriging, however their spatial density is the lowest on average. We conclude that the large number and the accuracy of the opportunistic sensors lead to a better interpolation.

The block kriging approach in the interpolation framework accounts for the integral characteristic of the CMLs. The comparison to kriging with the center of each CML as point measurement (CML_point_{int}) done in the same manner as in Fig. 3 shows a higher PCC for the block kriging approach (see Fig. A2). For temporal aggregations, of one and two hours CML_point_{int} leads to higher KGE values. With the variance directly affecting KGE values, we assume that the reduced variance in CML_{int} of block kriging is the reason for the lower KGE values.

4.2. *Performance of interpolated rainfall products compared to gauge datasets on different scales*

The performance of the interpolated datasets is analyzed for the whole of Germany, a regional, and a local subset with different, independent reference datasets. Additionally, two radar datasets from the DWD are compared analogously to the reference data.

4.2.1. *Country-wide, daily scale for Germany*

For the country-wide scale we used data from manual rain gauges with a daily resolution from the DWD (DWD_{man}). The interpolated rainfall maps and radar product values for this evaluation are taken at the respective grid cell of the locations of DWD_{man}

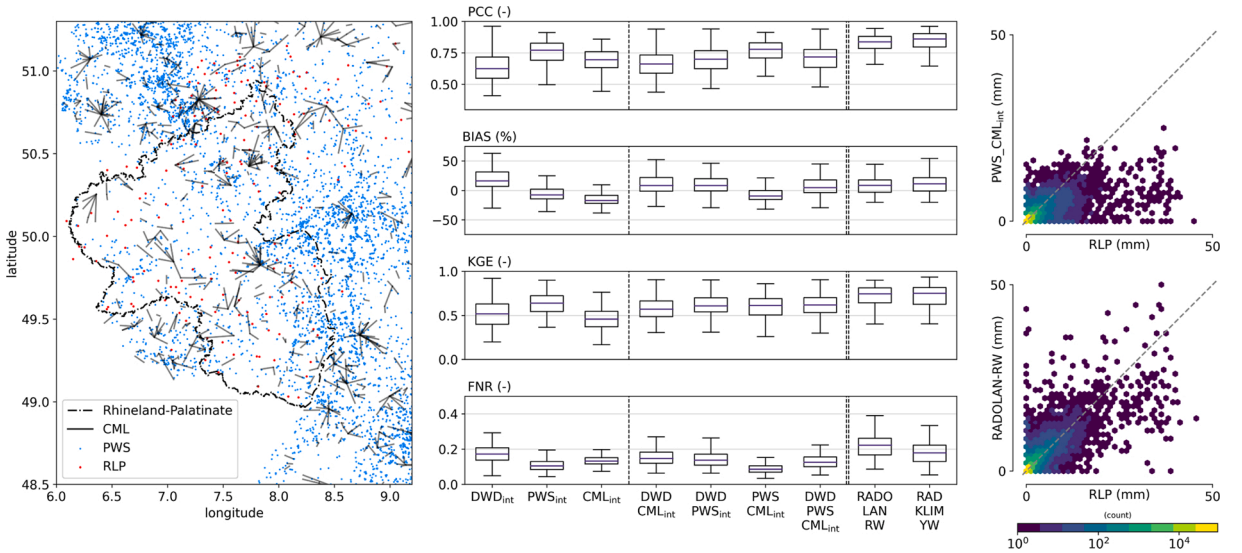

Fig. 5. Map of Rhineland-Palatinate and surroundings with Rhineland-Palatinate gauges (reference), PWS locations and CML paths, boxplots of performance measures for the seven interpolated products as well as RADOLAN-RW and RADKLIM-YW against the reference. Dashed lines are similar to Fig. 4. On the right, scatter density plots of hourly PWS_CML$_{int}$ and RADOLAN-RW rain sums are compared to the reference.

gauges. An overview of the DWD$_{man}$ gauges, PWSs locations and CMLs is given in the map of Fig. 4 together with results of the evaluation for this scale.

In general, the radar products match the reference data better than the interpolated products. They have slightly higher PCC and KGE as well as a lower FPR. The comparison is not quite fair, though. The radar products are based on measurements directly at each reference station's location while the interpolated rainfall fields have to rely on observations at a certain distance, a distance that varies from hundreds of meters to tens of kilometers in the north-eastern part of Germany. Nevertheless, the performance measures of the interpolated products are good. Looking at the two radar products, RADKLIM-YW outperformed RADOLAN-RW except for FPR. This leads to the assumption that the climatological adjustments of RADKLIM-YW, e.g. seasonal correction of range dependent underestimation, improve this radar product not only for longer aggregations times, from which the climatological corrections are derived, but also on a daily scale.

Among the interpolated products, the ones including PWSs compared better to the reference than the others. The worst performance was obtained by CML$_{int}$. These results are in accordance with the cross validation. The scatter density plots show all daily rainfall values for PWS_CML$_{int}$ and RADOLAN-RW against DWD$_{man}$. The number of missed rainy days (false negative rate: FNR) from the reference, visible along the x-axis in Fig. 4, was lower for the interpolated product than for the radar product.

The performance of PWS$_{int}$ and the other combinations with PWSs is better compared to the DWD$_{auto}$ product. The reason for this is the high spatial density resulting from the high number of OS. This is true even though the OS are heterogeneously distributed in contrast to the more homogeneously distributed DWD$_{man}$. This means that hydrological modeling studies, which often use data from rain gauge networks, can benefit from rainfall information derived from opportunistic sensors. Requirements for such applications are the availability of opportunists sensors, the acquisition of their data and a thorough quality control.

Similar to the cross validation, the subset of DWD$_{man}$ surrounded by the densest opportunistic network were examined separately (see Fig. A3). The results differ only slightly from the country-wide analysis of Fig. 4. The range of the individual performance measures are more narrow and PWS$_{int}$ and CML$_{int}$ have a small improvement, similar to what was observed for the daily aggregation results of the cross validation. This means that the density of opportunistic sensors is sufficient for rainfall mapping in almost all parts of Germany except for the north-eastern part of Germany.

4.2.2. Regional, hourly scale for Rhineland-Palatinate

As reference on a regional scale 169 rain gauges with an hourly resolution operated by the State Agrometeorological Agency of Rhineland-Palatinate (RLP) are used. An overview of the Rhineland-Palatinate gauges, PWS locations and CMLs is given in the map of Fig. 5 together with results of the evaluation for this scale. For the PCC all interpolated products with opportunistic sensors outperformed the DWD$_{int}$ product. PWS$_{int}$ and the other combinations with PWSs performed almost as good as the radar products. The combination PWS_CML$_{int}$ reached marginally higher PCC values than PWS$_{int}$. CML$_{int}$ has the highest (negative) bias. This can be caused for example by the integral character of the CMLs underestimating the highest rainfall events and the heterogeneous distribution of the CMLs. The FPR (not shown in the plot for the evaluation at this scale) of all products is 5 times smaller than FNR, with the best performance for PWS$_{int}$ and PWS_CML$_{int}$. RADOLAN-RW shows more over- and underestimation of the highest hourly rainfall events which can be seen in the scatter plot. The PWS_CML$_{int}$ product underestimates the highest rainfall events, which could be caused by a combination of the effect of the integral character of the CML measurement and the smoothing of the field caused by the 10 % nugget

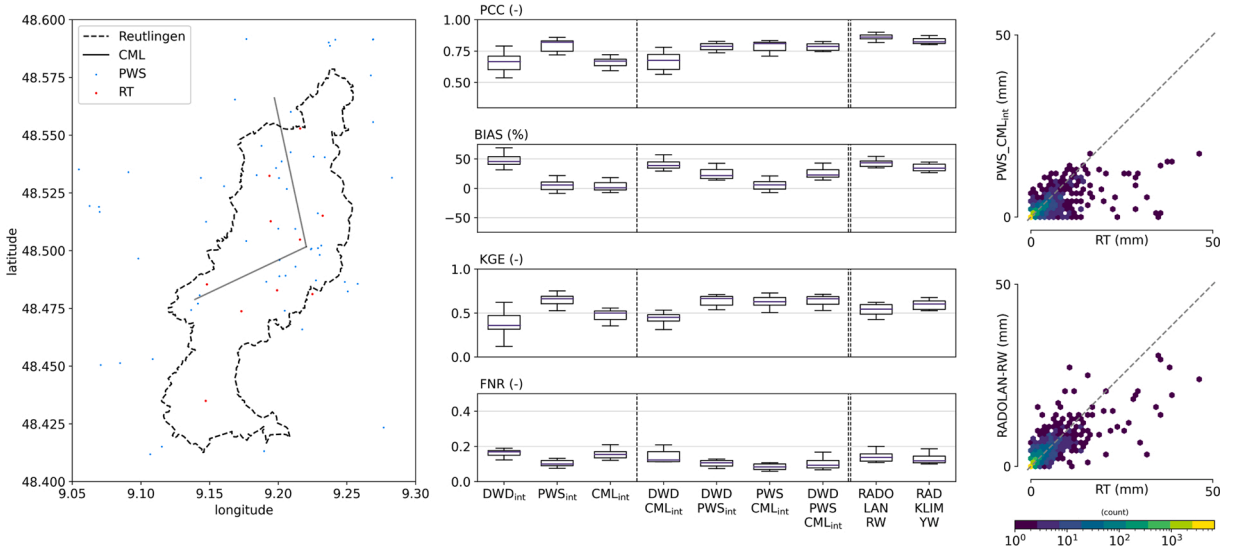

Fig. 6. Map of Reutlingen with Reutlingen gauges (reference), PWS locations and CML paths, boxplots of performance measures for the seven interpolated products as well as RADOLAN-RW and RADKLIM-YW against the reference. Dashed lines are similar to Fig. 4. On the right, scatter density plots of hourly PWS_CML$_{int}$ and RADOLAN-RW rain sums are compared to the reference.

that is used in Kriging to represent the uncertainty of the opportunistic sensors. Moreover, despite the thorough PWSs quality check, there could still be some stations that were not filtered and that recorded false zeros for the intense events affecting the performance of the interpolation products.

The biggest difference to the country-wide DWD$_{man}$ reference evaluation is that the comparison to RLP is based on an hourly resolution. On this temporal resolution, rainfall shows more variability than on a daily scale. Hence, on the hourly scale all interpolated and radar products have lower values for PCC and KGE. Nevertheless, the agreement of the best performing interpolation products with the reference data is high. It can be assumed that for all regions with similar distribution and density of opportunistic sensors in Germany, similar results as for Rhineland-Palatinate could be achieved. That means, opportunistic sensors can provide rainfall estimates with a good quality for most parts of Germany, with the exception of north-eastern regions where their network density is low, on an hourly scale.

4.2.3. Local, hourly scale for the city of Reutlingen

Ten rain gauges operated by the city of Reutlingen (RT) are used to evaluate the performance of the interpolated products and radar datasets on a local scale with a temporal resolution of one hour. An overview of the RT gauges, PWS locations and CMLs is given in the map of Fig. 6 together with results of the evaluation for this scale. The network of 10 rain gauges in and around Reutlingen has a significantly higher density than the previous gauge datasets used as reference. On this small scale, the high number of PWSs in this urban area becomes apparent, with around thirty stations in Reutlingen. PWS$_{int}$ and the combinations with PWSs compared best to the reference with a high PCC. CML$_{int}$ and combinations reproduce the reference rainfall values slightly better than DWD$_{int}$. DWD$_{int}$ as well as the radar products show a positive bias. The reason could be the large distance of the next rain gauge which is also used to adjust the radar products. The next rain gauges on this local scale are more than 15 *km* away and not located in the area shown by Fig. 6. This could make a difference in the rather complex terrain at the border of the Swabian Alps. For the OS products the bias is almost zero. For the most intense events shown in the scatter plot of PWS_CML$_{int}$ the opportunistic sensors are underestimated by the interpolated product. Upon closer inspection all reference rainfall points above 20 *mm* were from an event on the 12th of June 2018 lasting 3 hours. While some of the PWSs resembled the reference gauges rainfall almost perfectly, others underestimated this event by a factor of ten. The two CMLs also underestimated the peak rainfall due to a complete loss of signal for a total of 12 and 21 minutes, respectively. We currently do not interpolate or fill gaps of this size in our processing. The rainfall sum of the hour with this data gap is treated as missing value. Hence, the one hour with the peak rainfall sum is missing from the CML data. This rainfall event is an interesting opportunity to study the ability and required processing steps to measure intense events with PWSs and CMLs in the future. First steps in this direction could be the improvement of the event based filter for PWSs or filling CML outages caused by rain with the maximum of measurable rainfall at this CML.

Apart from the city of Reutlingen, there are few cities which operate such a dense and high quality network of rain gauges. Only with such a dense network of conventional rain gauges, we were able to evaluate the performance of opportunistic sensors on such a small scale. The opportunistic sensors show very good results in estimating rainfall on this local scale, therefore we conclude that rainfall information from PWSs and CMLs are highly valuable for the rainfall estimation in other urban areas with few or no conventional rain gauges. This opens the possibility to use opportunistic rainfall sensors for applications in urban hydrology for all cities with a similar density of opportunistic sensors.

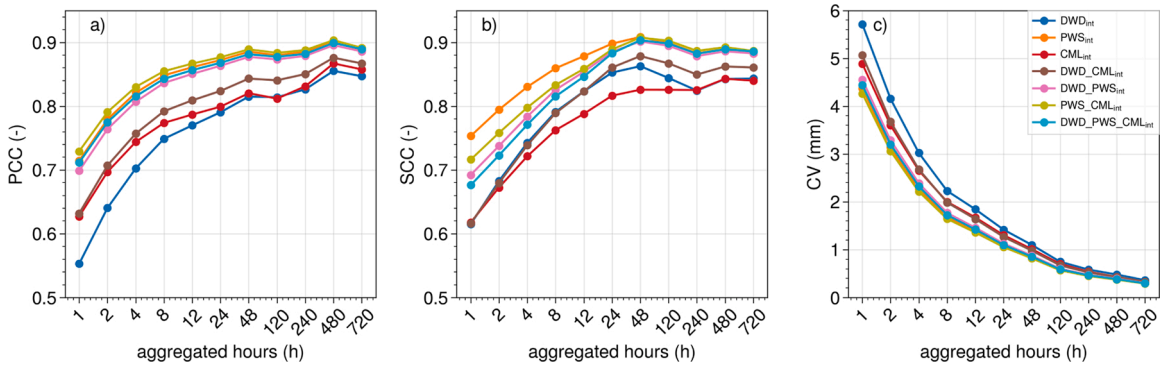

Fig. 7. Performance measures of the cross validation for the 0.99 quantile of rain events for each temporal aggregation.

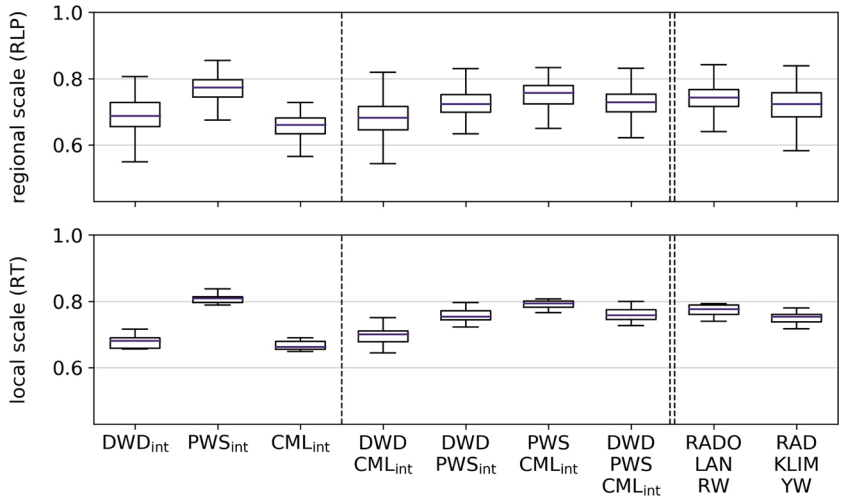

Fig. 8. Spearman's rank correlation coefficient of interpolated products and radar products against the hourly references of Rhineland-Palatinate (regional scale), and Reutlingen (local scale).

4.3. Performance for high intensity rainfall

We investigated the potential of opportunistic sensors in capturing the most intense rain events with the leave one out cross validation results. We performed the same analysis as in Section 4.1 but only considered rain events above the 0.99 quantile level of each aggregation interval. The results in Fig. 7 show PCC, Spearman's rank correlation coefficient (SCC) and CV. The SCC defined in Appendix C is used here because it credits the skewed distribution of rainfall. For the PCC and CV the results are similar to the cross validation results for all rain events. PWS_{int} and combinations with PWSs performed best, while the combination of PWSs and CMLs was the overall best. CML_{int} also outperformed DWD_{int} for these two measures. Considering the SCC, the best results were obtained from PWS_{int} without further combination. Both CML and DWD data could not add further information to increase the SCC. One reason for this might be the increased distance between CML and especially DWD sensors opposed by the high density of PWSs. For the SCC, DWD and CML performed similarly for one hour while DWD reaches higher values for aggregations between two and 120 hours.

For an analysis of the performance of the interpolated products and radar datasets for high intensity rainfall for the regional and local scale we show the SCC for hourly rainfall sums in Fig. 8. The German-wide scale is not shown as it is only available with a daily temporal resolution and an hourly evaluation for the whole of Germany is already covered by Fig. 7.

The three individual interpolated products show similar results, on both scales. As in Fig. 7, PWS_{int} shows the overall highest SCC while DWD_{int} reaches slightly higher values than CML_{int}. The combined interpolated products show a similar SCC as the radar products, except for DWD-CML_{int}. This again highlights the potential of exploiting dense opportunistic sensor networks on both regional and urban scales for hydrometeorologic purposes. For the radar products, the climatological adjustment seems to increase the SCC marginally.

The lower SCC values for CML_{int} on both scales could be caused by several reasons. One reason for this is the engineering requirements of the CML network which allows an outage of the systems during the strongest rainfall events for some minutes. This results in a maximum rain rate before signal loss between 40 mmh^{-1} and more than 150 mmh^{-1}, depending on the exact CML configuration (length, frequency, transmit power, antenna gain). Thus, for heavy rainfalls, CMLs do not always provide accurate

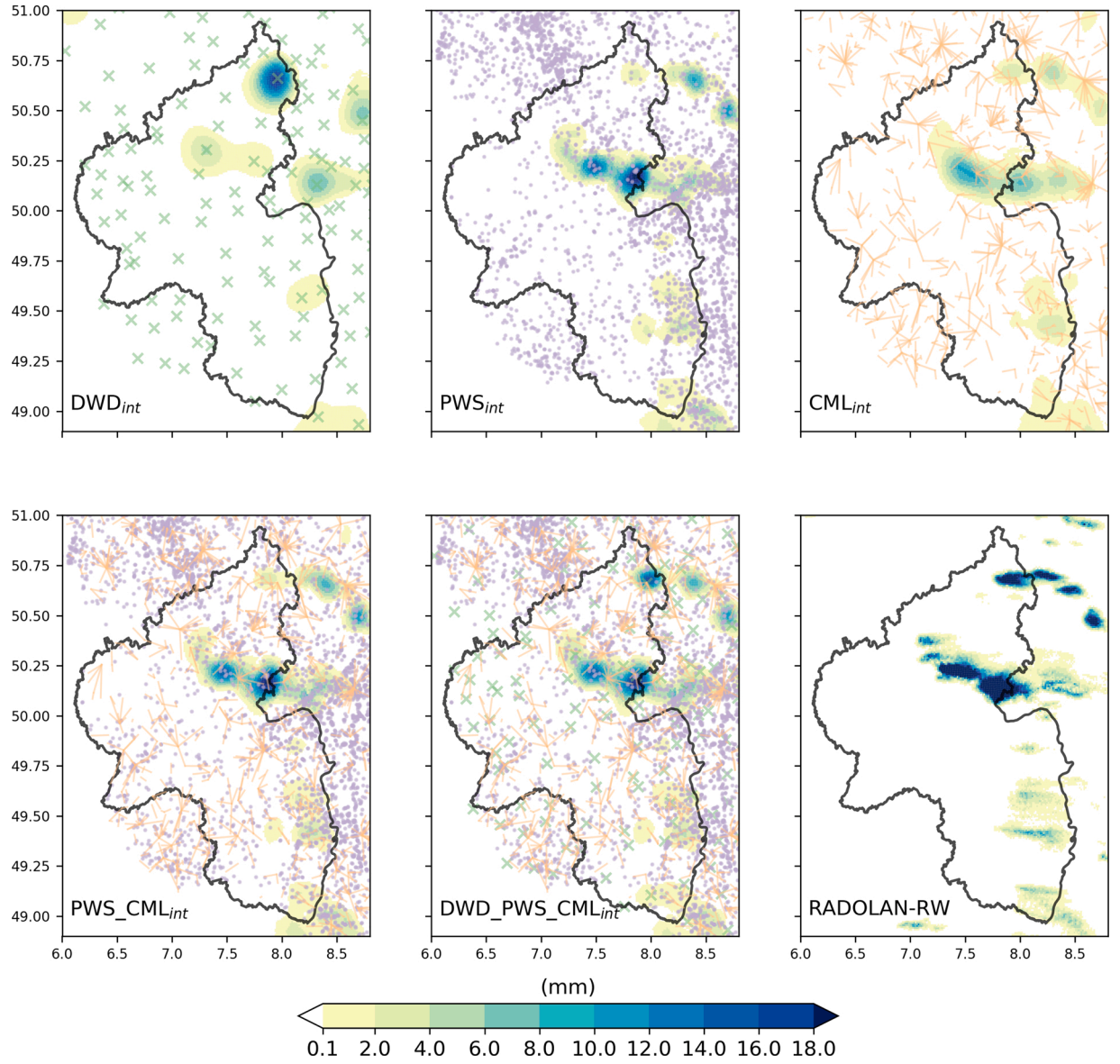

Fig. 9. Rainfall example maps for one hour accumulated rainfall at 12.07.2019 12:00 CET for three different interpolation products, a radar product and their differences between each other.

rainfall information. Consequently, the rank correlation for high rain intensities could be decreased for CMLs. Another reason is the integral character of the CML measurements which gives the path-averaged rain rate independently of the distribution of rain rates along the CMLs path. This leads to an underestimation of the highest rain rates along the path. Finally, the effect of the classification of rainy and dry periods in the CMLs processing has to be considered. Every wrong classification which can be caused by non-rain induced attenuation, multi-path propagation or others, will influence the FPR and FNR which ultimately have a large influence on the SCC. Considering all this, the hourly SCC of CML_{int} is still close to the one of the conventional rain gauge product DWD_{int}.

4.4. Rain event example in Rhineland-Palatinate

To illustrate the interpolation framework results for the different datasets we show an example for several interpolated rainfall maps from different combinations and RADOLAN-RW in Rhineland-Palatinate in Fig. 9. On 12 July 2019 at 12:00 several rain cells are visible for all interpolation products and RADOLAN-RW. For some regions, the DWD_{auto} network misses rainfall because the station density is too sparse. This can be seen in the map showing the opportunistic sensors and DWD_{auto} stations locations. For DWD_{int} the underlying structure of the network is clearly visible. In comparison, PWS_CML_{int} shows more variability in the rainfall field and with most features related to several opportunistic sensors. The opportunistic sensors miss the most intense feature measured by the

DWD_{auto} gauges in the north of Rhineland-Palatine, while PWS_{int} has the highest intensities further south. We presume that the increased variability due to the larger number of measurements should be closer to the true spatio-temporal distribution of rainfall. Most features and structures detected by RADOLAN-RW are visible in PWS_CML_{int}, while the radar product produces higher rainfall values. It seems that more (opportunistic) sensors lead to higher spatial variability in the interpolated rainfall fields, which could potentially improve hydrological applications.

5. Conclusion

The study region of Germany with two sub-regions, namely the state of Rhineland-Palatinate and the city of Reutlingen, are hydrometeorologically well monitored compared to most locations in the world and therefore provide a suitable testing ground to evaluate opportunistic rainfall sensors. In this study, we demonstrate the use of two different types of such opportunistic sensors. We obtain rainfall fields using a geostatistic interpolation framework incorporating block kriging from point information of PWSs and line information of CMLs. Seven combinations of CML, PWS and official hourly rain gauge data from the DWD are evaluated for three different reference datasets in three study regions. Two radar products from the DWD were evaluated in the same manner as the interpolated datasets to further quantify the performance of the interpolated rainfall maps.

Both PWS and CML data come with individual drawbacks, e.g. unfavorable locations of PWSs or erratic fluctuations in the raw CML data. After the respective data retrieval and the rainfall estimation for the CMLs, both datasets are filtered with an indicator correlation and event based method and are bias corrected. Only then, they are used in different combinations with and without hourly rain gauge data from the DWD for interpolation. While the presented indicator correlation filter approach relies on a primary station network, the data from this network could potentially come from another period as the rain rates are compared and adjusted only by their distribution functions. Besides very high rainfall events, i.e. with return periods of several years, the rainfall distribution for individual years as used in this study might not change this distribution too much. Hence, this approach could be usable for opportunistic sensors in areas where the number of rain gauges was reduced over the last decades because only their distribution function is needed.

To use the indicator correlation filter, event based filter and the bias correction for data with higher temporal resolution than one hour, upcoming issues like the increasing number of zero precipitation events and the filtering of small-scaled extreme events which were not observed by the primary network (i.e. DWD gauges), have to be addressed. Potential solutions could be the usage of advection vectors or the mutual filtering of PWS and CML, where one opportunistic sensor can serve as primary network for the other and vice versa. In this study, reliable CMLs were identified using the indicator correlation and event based filter and their values were corrected using the bias correction method. These methods accounted for the line characteristic of the CMLs measurement.

A cross validation shows the ability of CMLs and especially PWSs for rainfall mapping. This is true for hourly as well as for multi-day aggregations. The opportunistic sensors are able to produce reasonable rainfall maps with increased spatial variability compared to rainfall maps derived from conventional rain gauge data. These rainfall maps were evaluated country-wide for Germany with independent daily gauge data as reference and for Rhineland-Palatinate and Reutlingen with hourly gauge data as reference. To set the results of the evaluation in a perspective we used the official gauge adjusted radar datasets RADOLAN-RW and RADKLIM-YW from the DWD.

On the country-wide daily scale the radar products had a better agreement with the reference than the interpolated products. For the two sub-regions with an hourly resolution, the interpolated products performed similarly good as the radar products. The high number of opportunistic sensors might be the most import reason for this. Differences between the interpolated and radar products can be found especially for the highest rainfall amounts. Overall, interpolations incorporating PWS data performed best while the usage of CMLs resulted in better performance metrics as product from hourly DWD rain gauges. Similar results were found for the most intense rain events with the exception of CMLs which performed worse than the DWD product for temporal aggregations of several hours.

The results show the accuracy and increased spatial variability of rainfall maps from opportunistic sensors, especially on smaller spatial and temporal scales. Numerous hydrometeorological applications can potentially benefit from this information. The almost instantanous data availability could be used to access real-time rainfall information. Applications in urban hydrology could therefore benefit both from the potential real-time accessibility and the often dense opportunistic sensor networks in this urban areas. Nevertheless, some of the presented methods, e.g. the indicator correlation filter, cannot readily be used for real-time applications but rather provide a baseline for such developments. Another opportunity is the combination with traditional gauge or radar datasets to derive a further improved joint product that leverages the individual advantages of all individual traditional and opportunisitc sensors.

Authors statement

Maximilian Graf: Conceptualization, Methodology, Software, Writing – Original Draft, Writing – Review & Editing, Visualization.
Abbas El Hachem: Methodology, Software, Writing – Original Draft, Writing – Review & Editing, Visualization.
Micha Eisele: Methodology, Software, Data Curation, Writing – Original Draft, Writing – Review & Editing, Visualization.
Jochen Seidel: Conceptualization, Writing – Original Draft, Writing – Review & Editing.
Christian Chwala: Conceptualization, Data Curation, Writing – Original Draft, Writing – Review & Editing.
Harald Kunstmann: Funding Acquisition, Conceptualization, Supervision.
András Bárdossy: Conceptualization, Methodology, Software, Writing – Original Draft, Writing – Review & Editing, Supervision.

Conflict of interest

The authors certify that they have no affiliations with or involvement in any organization or entity with any financial interest (such

as honoraria; educational grants; participation in speakers' bureaus; membership, employment, consultancies, stock ownership, or other equity interest; and expert testimony or patent-licensing arrangements), or non-financial interest (such as personal or professional relationships, affiliations, knowledge or beliefs) in the subject matter or materials discussed in this manuscript.

Declaration of Competing Interest

The authors report no declarations of interest.

Acknowledgements

We are grateful to Ericsson providing the CML data, and especially to Reinhard Gerigk, Michael Wahl, and Declan Forde for their ongoing support and cooperation. We would like to thank the State Agrometeorological Agency Rhineland-Palatinate, the State Environmental Agency Rhineland-Palatinate, and the SER Reutlingenfor providing the corresponding precipitation data. We also would like to thank the German Weather Service for providing rain gauge and radar data. This work was co-funded by the Helmholtz Association of German Research Centreswithin the "Digital Earth" project. We acknowledge support by the KIT-Publication Fund of the Karlsruhe Institute of Technology. We further want to thank two reviewers for their thorough work.

Appendix A. Additional Figures

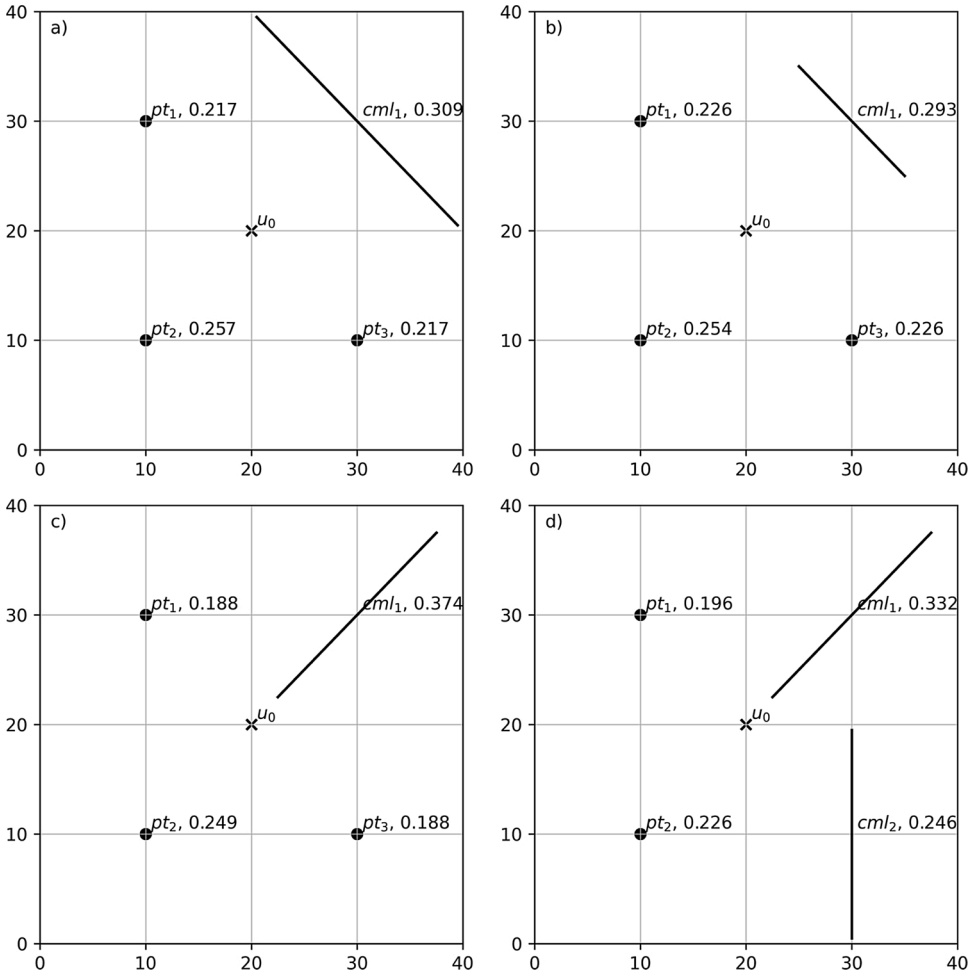

Fig. A1. Different weights w^T for points (pt_i) and line segments (cml_i) depending on their length and orientation for estimating the precipitation amount at a given location u_0. If the center of the CMLs in each of these four examples (a–d) were assumed to be point information, the weights of all points would be equal (here: 0.25). However, if the length and orientation of the CMLs are taken into account, different weights are obtained.

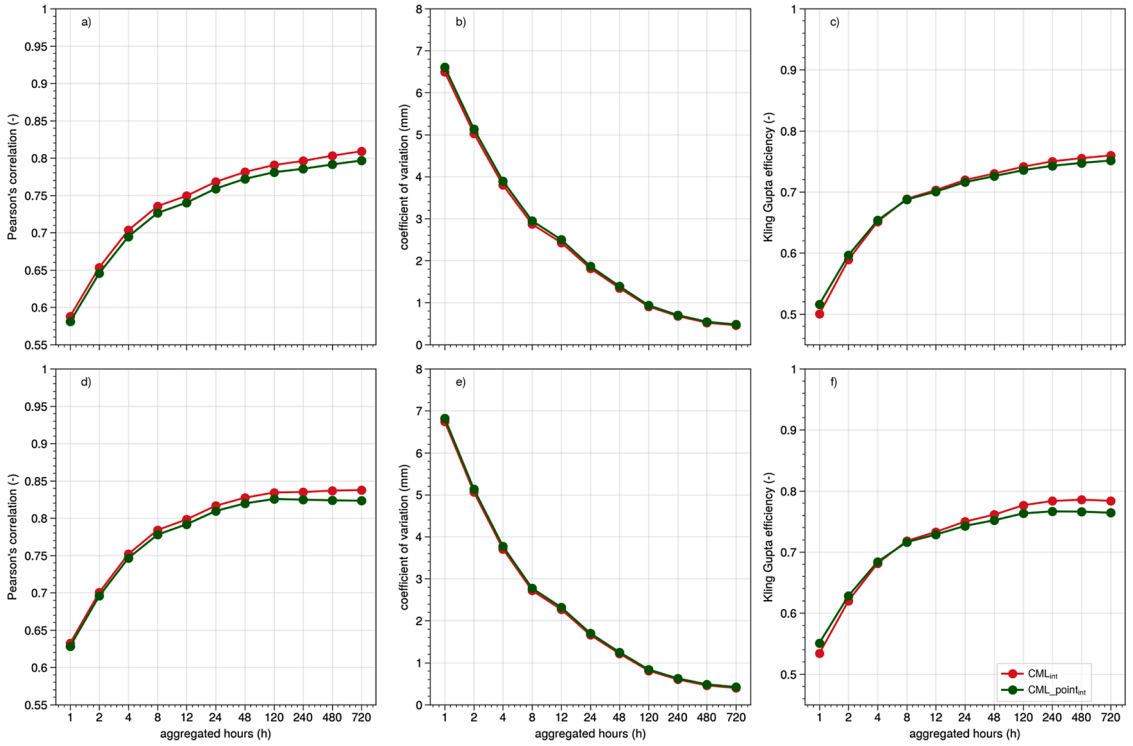

Fig. A2. Performance measures of the cross validation results from the interpolation framework for different temporal aggregations. Here CML_{int} and CML_point_{int} are shown. For CML_point_{int} the points at the center of each CML were used as point information in the interpolation framework. (a) to (c) show PCC, CV and KGE for country-wide validation stations and (d) to (f) show PCC, CV and KGE for validation stations with more than 80 PWSs or CMLs in 20 *km* vicinity. Those are the 10 percent of the validation station which are surrounded by the most opportunistic sensors.

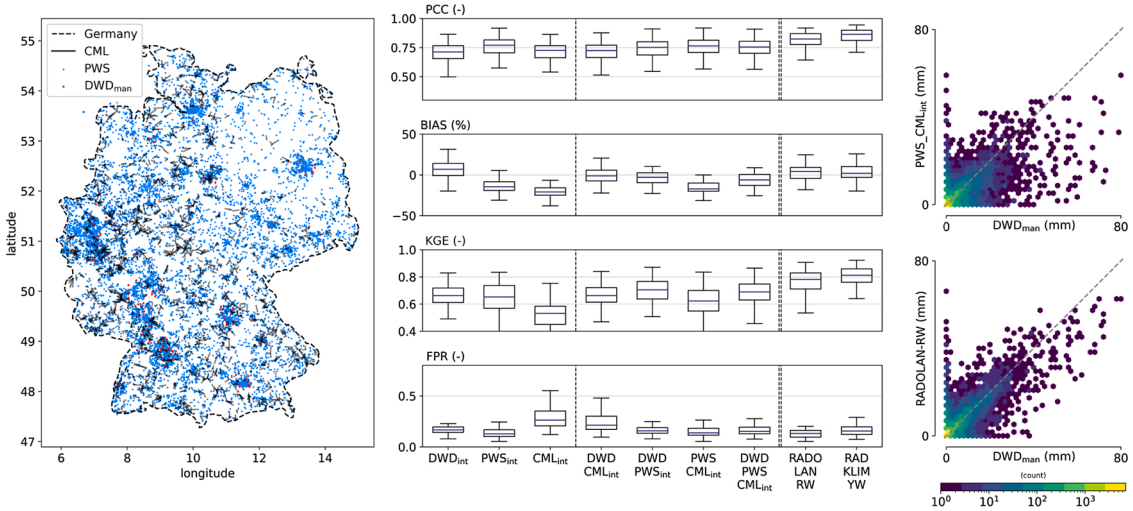

Fig. A3. Map of Germany with a subset of DWD_{man} gauges (reference), PWS locations and CML paths, boxplots of performance measures for the seven interpolated products as well as RADOLAN-RW and RADKLIM-YW against the reference, and scatter density plots of daily PWS-CML and RADOLAN-RW rain sum compared to the reference. The subset of DWD_{man} gauges compromises the 10 % of gauges which are surrounded by the most opportunistic sensors.

Appendix B. Consideration of the CML length for the indicator correlation filter and bias correction

It is well known that the length, area or volume of an observation or measurement has an effect on the statistical properties of this observation. This so-called support effect has been intensively studied in geostatistics, mainly for mining applications. There are several approaches which can be used to calculate the change of variance as a function of the support size and the variogramm. Block

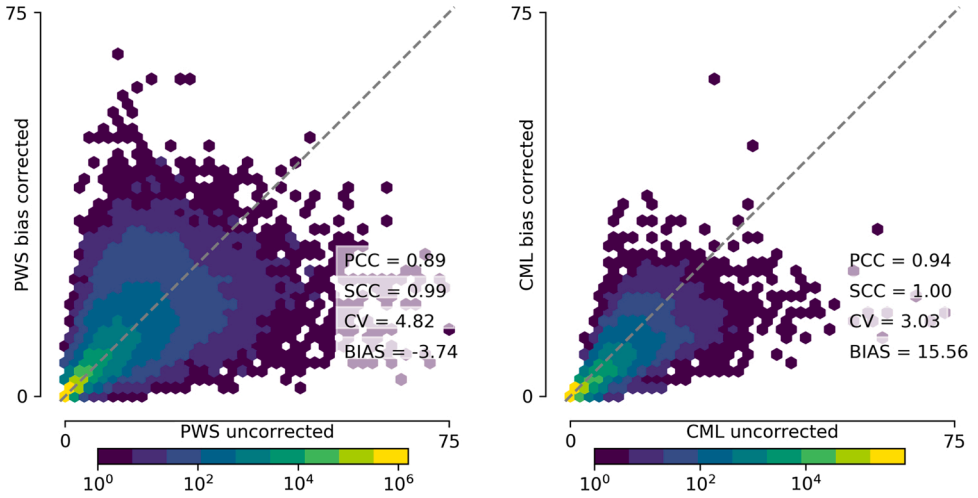

Fig. B1. Comparison of uncorrected and bias corrected hourly PWS and CML rain rates.

Kriging, as applied in this paper is also taking the support size into account.

The different lengths of the CMLs have to be taken into account for the application of the indicator correlation filter and the bias correction. The classical geostatistical formulas cannot be used, as we consider the distribution of the values and not only their variances. Therefore, the following simulation based approach is considered.

The indicator correlation between the CML and a primary station is partly influenced by the orientation and the length of the CML. As the indicator correlation is independent of the marginal distribution only the dependence structure is of importance.

It is assumed that the spatial dependence of precipitation follows a normal copula. This is a frequent assumption, however not often stated explicitly.

This means that precipitation $Z(x,t)$ can be obtained from the realization of a spatially stationary normal process $Y(x,t)$ by a transformation:

$$Z(x,t) = F_x^{-1}(\Phi(Y(x,t)))$$

where $F_x()$ is the distribution function of precipitation for location x and $\Phi()$ is the distribution function of the standard normal distribution.

$$Z(L,t) = \frac{1}{|L|}\int_L Z(y,t) \ \ \mathrm{dy}$$

From the point observations the spatial correlation function of the indicators can be calculated. This can be transformed to a correlation function of a normal Y $C_Y(h)$. With this correlation function realizations of Y can be simulated, and with the local distributions $F_y()$ realizations of $Z(x,t)$ and $Z(L,t)$ can be derived. Thereafter, the indicator correlations, and the distribution functions $F_L()$ of $Z(L,t)$ can be calculated. These distribution function can also be used for bias correction of the CMLs.

For the indicator correlations a good approximation can be obtained by replacing the line L by a specific point u, such that:

$$C_I(x,L) = C_I(x,u)$$

where

$$d(x,u) = d(x,L) = \frac{1}{L}\int_L d(x,y) \ \ \mathrm{dy}$$

This means that for the indicator correlation filter which for CMLs with a primary network the CMLs have to be considered as $d(x,L)$ and not as the central point along its path L.

The same assumption can be used for the bias correction. To calculate the distribution of $Z(L,t)$ as a first step the distribution functions of the precipitation observations at the primary observations are interpolated for each point y of the line L (in practice L is discretized to a few points). This is done the same way as for the PWSs. Using these simulations the line averages can be calculated as follows:

$$Z(L,t) = \frac{1}{|L|}\int_L Z(y,t) \ \ \mathrm{dy} = \frac{1}{|L|}\int_L F_y^{-1}(\Phi(Y(y,t))) \ \ \mathrm{dy}$$

So a Monte Carlo simulation of Y can be used to obtain the distribution function of $Z(L,t)$. Due to the averaging procedure this distribution is different from the point distributions. For example, the probability of high values is reduced. Fig. B1 shows the result of

the bias correction for hourly rain rates.

Appendix C. Diagnostic values considered in this study

Here all used diagnostic values are described. The values which are evaluated (e.g. interpolated values from DWD_PWS_CML$_{int}$) are denoted as pred while the values from the references are denoted as ref. std refers to the standard deviation.

Pearson's correlation coefficient (PCC)

$$\mathrm{PCC} = \frac{\sum_{i=1}^{n}(\mathrm{pred}_i - \overline{\mathrm{pred}})(\mathrm{ref}_i - \overline{\mathrm{ref}})}{\sqrt{\sum_{i=1}^{n}(\mathrm{pred}_i - \overline{\mathrm{pred}})^2(\mathrm{ref}_i - \overline{\mathrm{ref}})^2}}$$

Coefficient of variation (CV)

$$\mathrm{CV} = \frac{\mathrm{std}\sum(\mathrm{pred} - \mathrm{ref})}{\overline{\mathrm{ref}}}$$

Kling-Gupta efficiency (KGE)

$$\mathrm{KGE} = 1 - \sqrt{(r-1)^2 + (\alpha - 1)^2) + (\beta - 1)^2}$$

where r = PCC(pre,ref) and

$$\alpha = \frac{std(pred)}{std(ref)}$$

and

$$\beta = \frac{\overline{pred}}{\overline{ref}}$$

Spearman's rank correlation coefficient

$$\mathrm{SCC} = 1 - \frac{6\sum_{i=1}^{n} d_i^2}{n(n^2-1)}$$

where

$$d_i = \mathrm{rg}(\mathrm{pred}_i) - \mathrm{rg}(ref_i)$$

and n is the number of considered time steps.

Bias

$$\mathrm{bias} = \frac{\overline{(\mathrm{pred} - \mathrm{ref})}}{\overline{\mathrm{ref}}}$$

Appendix D. Supplementary Data

Supplementary data associated with this article can be found, in the online version, at https://doi.org/10.1016/j.ejrh.2021.100883.

References

Allamano, P., Croci, A., Laio, F., 2015. Toward the camera rain gauge. Water Resour. Res. 51, 1744–1757. https://doi.org/10.1002/2014WR016298. URL https://agupubs.onlinelibrary.wiley.com/doi/abs/10.1002/2014WR016298. _eprint: https://agupubs.onlinelibrary.wiley.com/doi/pdf/10.1002/2014WR016298.

Andersson, J., Berg, P., Hansryd, J., Jacobsson, A., Olsson, J., Wallin, J., 2017. Microwave links improve operational rainfall monitoring in Gothenburg, Sweden. Proc. CEST. Proc. CEST.

Atlas, D., Ulbrich, C.W., 1977. Path- and area-integrated rainfall measurement by microwave attenuation in the 1-3 cm band. J. Appl. Meteorol. 16, 1322–1331. URL https://journals.ametsoc.org/doi/abs/10.1175/1520-0450 doi:10.1175/1520-0450(1977)016<1322:PAAIRM>2.0.CO;2.

Balsamo, G., Agusti-Panareda, A., Albergel, C., Arduini, G., Beljaars, A., Bidlot, J., Blyth, E., Bousserez, N., Boussetta, S., Brown, A., Buizza, R., Buontempo, C., Chevallier, F., Choulga, M., Cloke, H., Cronin, M.F., Dahoui, M., De Rosnay, P., Dirmeyer, P.A., Drusch, M., Dutra, E., Ek, M.B., Gentine, P., Hewitt, H., Keeley, S.P. E., Kerr, Y., Kumar, S., Lupu, C., Mahfouf, J.-F., McNorton, J., Mecklenburg, S., Mogensen, K., Muñoz-Sabater, J., Orth, R., Rabier, F., Reichle, R., Ruston, B., Pappenberger, F., Sandu, I., Seneviratne, S.I., Tietsche, S., Trigo, I.F., Uijlenhoet, R., Wedi, N., Woolway, R.I., Zeng, X., 2018. Satellite and in situ observations for advancing global earth surface modelling: a review. Remote Sensing 10, 2038. https://doi.org/10.3390/rs10122038. URL https://www.mdpi.com/2072-4292/10/12/2038. Number: 12 Publisher: Multidisciplinary Digital Publishing Institute.

Bartels, H., Weigl, E., Reich, T., Lang, P., Wagner, A., Kohler, O., Gerlach, N., 2004. Routineverfahren zur Online-Aneichung der Radarniederschlagsdaten mit Hilfe von automatischen Bodenniederschlagsstationen(Ombrometer). Technical Report DWD.

Barthés, L., Mallet, C., 2013. Rainfall measurement from the opportunistic use of an Earth-space link in the Ku band. Atmospheric Measurement Techniques 6, 2181–2193. https://doi.org/10.5194/amt-6-2181-2013. URL https://amt.copernicus.org/articles/6/2181/2013/. Publisher: Copernicus GmbH.

van de Beek, R.C.Z., Olsson, J., Andersson, J., 2020. Optimal grid resolution for precipitation maps from commercial microwave link networks. Advances in Science and Research, pp. 79–85. https://doi.org/10.5194/asr-17-79-2020. Copernicus GmbH volume 17. URL https://asr.copernicus.org/articles/17/79/2020/. iSSN: 1992-0628.

Beek, R.C.Z..v.d, Olsson, J., Andersson, J., 2020. Optimal grid resolution for precipitation maps from commercial microwave link networks. Advances in Science and Research, pp. 79–85. https://doi.org/10.5194/asr-17-79-2020. Copernicus GmbH volume 17. URL https://asr.copernicus.org/articles/17/79/2020/. iSSN: 1992-0628.

Bell, S., Cornford, D., Bastin, L., 2013. The state of automated amateur weather observations. Weather 68, 36–41. https://doi.org/10.1002/wea.1980. URL https://rmets.onlinelibrary.wiley.com/doi/abs/10.1002/wea.1980. _eprint: https://rmets.onlinelibrary.wiley.com/doi/pdf/10.1002/wea.1980.

Berne, A., Delrieu, G., Creutin, J.-D., Obled, C., 2004. Temporal and spatial resolution of rainfall measurements required for urban hydrology. J. Hydrol. 299, 166–179. https://doi.org/10.1016/j.jhydrol.2004.08.002. URL http://www.sciencedirect.com/science/article/pii/S0022169404003634.

Berne, A., Krajewski, W.F., 2013. Radar for hydrology: unfulfilled promise or unrecognized potential? Adv. Water Resour. 51, 357–366. https://doi.org/10.1016/j.advwatres.2012.05.005. URL http://www.sciencedirect.com/science/article/pii/S0309170812001157.

Bárdossy, A., Seidel, J., El Hachem, A., 2021. The use of personal weather station observations to improve precipitation estimation and interpolation. Hydrol. Earth Syst. Sci. 25, 583–601. https://doi.org/10.5194/hess-25-583-2021. URL https://hess.copernicus.org/articles/25/583/2021/. Publisher: Copernicus GmbH.

Bronstert, A., Agarwal, A., Boessenkool, B., Crisologo, I., Fischer, M., Heistermann, M., Köhn-Reich, L., López-Tarazón, J.A., Moran, T., Ozturk, U., Reinhardt-Imjela, C., Wendi, D., 2018. Forensic hydro-meteorological analysis of an extreme flash flood: the 2016-05-29 event in Braunsbach, SW Germany. Sci. Total Environ. 630, 977–991. https://doi.org/10.1016/j.scitotenv.2018.02.241. URL http://www.sciencedirect.com/science/article/pii/S0048969718306405.

Båserud, L., Lussana, C., Nipen, T.N., Seierstad, I.A., Oram, L., Aspelien, T., 2020. TITAN automatic spatial quality control of meteorological in-situ observations. Adv. Sci. Res., pp. 153–163. https://doi.org/10.5194/asr-17-153-2020. Copernicus GmbH volume 17. URL https://asr.copernicus.org/articles/17/153/2020/. iSSN: 1992-0628.

Bundesnetzagentur, 2017. Bundesnetzagentur: Tätigkeitsbericht Telekommunikation 2016/2017, Tech. rep., Report 2016/2017, Bundesnetzagentur für Elektrizität, Gas, Telekommunikation, Post und Eisenbahnen, Bonn. URL https://www.bundesnetzagentur.de/SharedDocs/Downloads/DE/Allgemeines/Bundesnetzagentur/Publikationen/Berichte/2017/TB_Telekommunikation20162017.pdf?_blob=publicationFile&v=3.

Chwala, C., Keis, F., Kunstmann, H., 2016. Real-time data acquisition of commercial microwave link networks for hydrometeorological applications. Atmos. Meas. Tech. 9, 991–999. https://doi.org/10.5194/amt-9-991-2016. URL https://www.atmos-meas-tech.net/9/991/2016/.

Chwala, C., Kunstmann, H., 2019. Commercial microwave link networks for rainfall observation: assessment of the current status and future challenges. Wiley Interdiscip. Rev.: Water 6, e1337. https://doi.org/10.1002/wat2.1337. URL https://onlinelibrary.wiley.com/doi/abs/10.1002/wat2.1337.

Clark, M.R., Webb, J.D.C., Kirk, P.J., 2018. Fine-scale analysis of a severe hailstorm using crowd-sourced and conventional observations. Meteorol. Appl. 25, 472–492. https://doi.org/10.1002/met.1715. URL https://rmets.onlinelibrary.wiley.com/doi/abs/10.1002/met.1715. _eprint: https://rmets.onlinelibrary.wiley.com/doi/pdf/10.1002/met.1715.

Cristiano, E., ten Veldhuis, M.-C., van de Giesen, N., 2017. Spatial and temporal variability of rainfall and their effects on hydrological response in urban areas - a review. Hydrol. Earth Syst. Sci. 21, 3859–3878. https://doi.org/10.5194/hess-21-3859-2017. URL https://hess.copernicus.org/articles/21/3859/2017/. Publisher: Copernicus GmbH.

Doumounia, A., Gosset, M., Cazenave, F., Kacou, M., Zougmore, F., 2014. Rainfall monitoring based on microwave links from cellular telecommunication networks: first results from a West African test bed. Geophys. Res. Lett. 41, 6016–6022. https://doi.org/10.1002/2014GL060724. URL https://agupubs.onlinelibrary.wiley.com/doi/abs/10.1002/2014GL060724.

Emmanuel, I., Andrieu, H., Leblois, E., Flahaut, B., 2012. Temporal and spatial variability of rainfall at the urban hydrological scale. J. Hydrol. 430-431, 162–172. https://doi.org/10.1016/j.jhydrol.2012.02.013. URL http://www.sciencedirect.com/science/article/pii/S0022169412001126.

Fencl, M., Dohnal, M., Rieckermann, J., Bareš, V., 2017. Gauge-adjusted rainfall estimates from commercial microwave links. Hydrol. Earth Syst. Sci. 21, 617–634. https://doi.org/10.5194/hess-21-617-2017. URL https://www.hydrol-earth-syst-sci.net/21/617/2017/.

Fencl, M., Valtr, P., Kvičera, M., Bareš, V., 2019. Quantifying wet antenna attenuation in 38-GHz commercial microwave links of cellular backhaul. IEEE Geosci. Remote Sens. Lett. 16, 514–518. https://doi.org/10.1109/LGRS.2018.2876696. Conference Name: IEEE Geoscience and Remote Sensing Letters.

Graf, M., Chwala, C., Polz, J., Kunstmann, H., 2020. Rainfall estimation from a German-wide commercial microwave link network: optimized processing and validation for 1 year of data. Hydrol. Earth Syst. Sci. 24, 2931–2950. https://doi.org/10.5194/hess-24-2931-2020. URL https://www.hydrol-earth-syst-sci.net/24/2931/2020/. Publisher: Copernicus GmbH.

Haese, B., Hörning, S., Chwala, C., Bárdossy, A., Schalge, B., Kunstmann, H., 2017. Stochastic reconstruction and interpolation of precipitation fields using combined information of commercial microwave links and rain gauges. Water Resour. Res. 53, 10740–10756. https://doi.org/10.1002/2017WR021015. URL https://agupubs.onlinelibrary.wiley.com/doi/abs/10.1002/2017WR021015.

Hellmann, G., 1907. Die Niederschläge in den norddeutschen Stromgebieten. Nature 75, 556–557. https://doi.org/10.1038/075556a0. URL https://www.nature.com/articles/075556a0. Number: 1954 Publisher: Nature Publishing Group.

Jenkins, G., 2014. A comparison between two types of widely used weather stations. Weather 69, 105–110. https://doi.org/10.1002/wea.2158. URL https://rmets.onlinelibrary.wiley.com/doi/abs/10.1002/wea.2158. _eprint: https://rmets.onlinelibrary.wiley.com/doi/pdf/10.1002/wea.2158.

Jiang, S., Babovic, V., Zheng, Y., Xiong, J., 2019. Advancing opportunistic sensing in hydrology: a novel approach to measuring rainfall with ordinary surveillance cameras. Water Resour. Res. 55, 3004–3027. https://doi.org/10.1029/2018WR024480. URL https://agupubs.onlinelibrary.wiley.com/doi/abs/10.1029/2018WR024480. _eprint: https://agupubs.onlinelibrary.wiley.com/doi/pdf/10.1029/2018WR024480.

Kneis, D., Heistermann, M., 2009. Bewertung der Güte einer Radar-basierten Niederschlagsschätzung am Beispiel eines kleinen Einzugsgebiets. Hydrologie und Wasserbewirtschaftung. Hydrologie und Wasserbewirtschaftung 53, 160–171.

Kreklow, J., Tetzlaff, B., Kuhnt, G., Burkhard, B., 2019. A rainfall data intercomparison dataset of radklim, radolan, and rain gauge data for Germany. Data 4, 118. https://doi.org/10.3390/data4030118. URL https://www.mdpi.com/2306-5729/4/3/118.

Leijnse, H., Uijlenhoet, R., Stricker, J.N.M., 2007. Rainfall measurement using radio links from cellular communication networks. Water Resour. Res. 43 https://doi.org/10.1029/2006WR005631. URL https://agupubs.onlinelibrary.wiley.com/doi/abs/10.1029/2006WR005631.

van Leth, T.C., Overeem, A., Leijnse, H., Uijlenhoet, R., 2018. A measurement campaign to assess sources of error in microwave link rainfall estimation. Atmos. Meas. Tech. 11, 4645–4669. https://doi.org/10.5194/amt-11-4645-2018. URL https://www.atmos-meas-tech.net/11/4645/2018/.

Liberman, Y., Samuels, R., Alpert, P., Messer, H., 2014. New algorithm for integration between wireless microwave sensor network and radar for improved rainfall measurement and mapping. Atmos. Meas. Tech. 7, 3549–3563. https://doi.org/10.5194/amt-7-3549-2014. URL https://www.atmos-meas-tech.net/7/3549/2014/.

Lorenz, C., Kunstmann, H., 2012. The hydrological cycle in three state-of-the-art reanalyses: intercomparison and performance analysis. J. Hydrometeorol. 13, 1397–1420. URL https://www.jstor.org/stable/24914715. Publisher: American Meteorological Society.

Mahoney, W.P., O'Sullivan, J.M., 2013. Realizing the potential of vehicle-based observations. Bull. Am Meteorol. Soc. 94, 1007–1018. https://doi.org/10.1175/BAMS-D-12-00044.1. URL https://journals.ametsoc.org/view/journals/bams/94/7/bams-d-12-00044.1.xml. Publisher: American Meteorological Society Section: Bulletin of the American Meteorological Society.

McCabe, M.F., Rodell, M., Alsdorf, D.E., Miralles, D.G., Uijlenhoet, R., Wagner, W., Lucieer, A., Houborg, R., Verhoest, N.E.C., Franz, T.E., Shi, J., Gao, H., Wood, E.F., 2017. The future of Earth observation in hydrology. Hydrol. Earth Syst. Sci. 21, 3879–3914. https://doi.org/10.5194/hess-21-3879-2017. URL https://hess.copernicus.org/articles/21/3879/2017/. Publisher: Copernicus GmbH.

Meissner, D., Gebauer, S., Schumann, A.H., Rademacher, S., 2012. Analyse radarbasierter Niederschlagsprodukte als Eingangsdaten verkehrsbezogener Wasserstandsvorhersagen am Rhein. Hydrol. Wasserbewirtsch. 1 doi:10.5675/HyWa_2012,1_2.

Mercier, F., Barthés, L., Mallet, C., 2015. Estimation of finescale rainfall fields using broadcast tv satellite links and a 4DVAR assimilation method. J. Atmos. Oceanic Technol. 32, 1709–1728. https://doi.org/10.1175/JTECH-D-14-00125.1. URL https://journals.ametsoc.org/jtech/article/32/10/1709/4668/Estimation-of-Finescale-Rainfall-Fields-Using. Publisher: American Meteorological Society.

Messer, H., Zinevich, A., Alpert, P., 2006. Environmental monitoring by wireless communication networks. Science 312. https://doi.org/10.1126/science.1120034, 713–713, URL https://science.sciencemag.org/content/312/5774/713.

Ochoa-Rodriguez, S., Wang, L.-P., Gires, A., Pina, R.D., Reinoso-Rondinel, R., Bruni, G., Ichiba, A., Gaitan, S., Cristiano, E., van Assel, J., Kroll, S., Murlà-Tuyls, D., Tisserand, B., Schertzer, D., Tchiguirinskaia, I., Onof, C., Willems, P., ten Veldhuis, M.-C., 2015. Impact of spatial and temporal resolution of rainfall inputs on urban hydrodynamic modelling outputs: a multi-catchment investigation. J. Hydrol. 531, 389–407. https://doi.org/10.1016/j.jhydrol.2015.05.035. URL http://www.sciencedirect.com/science/article/pii/S0022169415003856.

Ostrometzky, J., Messer, H., 2018. Dynamic determination of the baseline level in microwave links for rain monitoring from minimum attenuation values. IEEE J. Sel. Top. Appl. Earth Obs. Remote Sens. 11, 24–33. https://doi.org/10.1109/JSTARS.2017.2752902. Conference Name: IEEE Journal of Selected Topics in Applied Earth Observations and Remote Sensing.

Overeem, A., Leijnse, H., Uijlenhoet, R., 2016a. Retrieval algorithm for rainfall mapping from microwave links in a cellular communication network. Atmos. Meas. Tech. 9, 2425–2444. https://doi.org/10.5194/amt-9-2425-2016. URL https://www.atmos-meas-tech.net/9/2425/2016/.

Overeem, A., Leijnse, H., Uijlenhoet, R., 2016b. Two and a half years of country-wide rainfall maps using radio links from commercial cellular telecommunication networks. Water Resour. Res. 52, 8039–8065. https://doi.org/10.1002/2016WR019412. URL https://agupubs.onlinelibrary.wiley.com/doi/abs/10.1002/2016WR019412.

Pollock, M.D., O'Donnell, G., Quinn, P., Dutton, M., Black, A., Wilkinson, M.E., Colli, M., Stagnaro, M., Lanza, L.G., Lewis, E., Kilsby, C.G., O'Connell, P.E., 2018. Quantifying and mitigating wind-induced undercatch in rainfall measurements. Water Resour. Res. 54, 3863–3875. https://doi.org/10.1029/2017WR022421. URL https://agupubs.onlinelibrary.wiley.com/doi/abs/10.1029/2017WR022421. _eprint: https://agupubs.onlinelibrary.wiley.com/doi/pdf/10.1029/2017WR022421.

Polz, J., Chwala, C., Graf, M., Kunstmann, H., 2020. Rain event detection in commercial microwave link attenuation data using convolutional neural networks. Atmos. Meas. Tech. 13, 3835–3853. https://doi.org/10.5194/amt-13-3835-2020. URL https://amt.copernicus.org/articles/13/3835/2020/. Publisher: Copernicus GmbH.

pycomlink (2021). URL https://github.com/pycomlink/pycomlink.

Rabiei, E., Haberlandt, U., Sester, M., Fitzner, D., 2013. Rainfall estimation using moving cars as rain gauges – laboratory experiments. Hydrol. Earth Syst. Sci. 17, 4701–4712. https://doi.org/10.5194/hess-17-4701-2013. URL https://hess.copernicus.org/articles/17/4701/2013/. Publisher: Copernicus GmbH.

Rios Gaona, M.F., Overeem, A., Raupach, T.H., Leijnse, H., Uijlenhoet, R., 2018. Rainfall retrieval with commercial microwave links in São Paulo, Brazil. Atmos. Meas. Tech. 11, 4465–4476. https://doi.org/10.5194/amt-11-4465-2018. URL https://www.atmos-meas-tech.net/11/4465/2018/.

Roversi, G., Alberoni, P.P., Fornasiero, A., Porcù, F., 2020. Commercial microwave links as a tool for operational rainfall monitoring in Northern Italy. Atmos. Meas. Tech. 13, 5779–5797. https://doi.org/10.5194/amt-13-5779-2020. URL https://amt.copernicus.org/articles/13/5779/2020/. Publisher: Copernicus GmbH.

Song, K., Liu, X., Zou, M., Zhou, D., Wu, H., Ji, F., 2020. experimental study of detecting rainfall using microwave links: classification of wet and dry periods. IEEE J. Sel. Top. Appl. Earth Obs. Remote Sens. 13, 5264–5271. https://doi.org/10.1109/JSTARS.2020.3021555. Conference Name: IEEE Journal of Selected Topics in Applied Earth Observations and Remote Sensing.

Tauro, F., Selker, J., Giesen, N.v.d., Abrate, T., Uijlenhoet, R., Porfiri, M., Manfreda, S., Caylor, K., Moramarco, T., Benveniste, J., Ciraolo, G., Estes, L., Domeneghetti, A., Perks, M.T., Corbari, C., Rabiei, E., Ravazzani, G., Bogena, H., Harfouche, A., Brocca, L., Maltese, A., Wickert, A., Tarpanelli, A., Good, S., Alcala, J.M.L., Petroselli, A., Cudennec, C., Blume, T., Hut, R., Grimaldi, S., 2018. Measurements and observations in the XXI century (MOXXI): innovation and multi-disciplinarity to sense the hydrological cycle. Hydrol. Sci. J. 63, 169–196. https://doi.org/10.1080/02626667.2017.1420191. URL https://doi.org/10.1080/02626667.2017.1420191.

Uijlenhoet, R., Overeem, A., Leijnse, H., 2018. Opportunistic remote sensing of rainfall using microwave links from cellular communication networks. Wiley Interdiscip. Rev: Water 5. https://doi.org/10.1002/wat2.1289. URL https://onlinelibrary.wiley.com/doi/abs/10.1002/wat2.1289.

Upton, G., Holt, A., Cummings, R., Rahimi, A., Goddard, J., 2005. Microwave links: the future for urban rainfall measurement? Atmos. Res. 77, 300–312. https://doi.org/10.1016/j.atmosres.2004.10.009. URL https://linkinghub.elsevier.com/retrieve/pii/S0169809505001079.

de Vos, L.W., Droste, A.M., Zander, M.J., Overeem, A., Leijnse, H., Heusinkveld, B.G., Steeneveld, G.J., Uijlenhoet, R., 2020. Hydrometeorological monitoring using opportunistic sensing networks in the amsterdam metropolitan area. Bull. Am. Meteorol. Soc. 101, E167–E185. https://doi.org/10.1175/BAMS-D-19-0091.1. URL https://journals.ametsoc.org/bams/article/101/2/E167/345054/Hydrometeorological-Monitoring-Using-Opportunistic. Publisher: American Meteorological Society.

de Vos, L.W., Leijnse, H., Overeem, A., Uijlenhoet, R., 2017. The potential of urban rainfall monitoring with crowdsourced automatic weather stations in Amsterdam. Hydrol. Earth Syst. Sci. 21, 765–777. https://doi.org/10.5194/hess-21-765-2017. URL https://hess.copernicus.org/articles/21/765/2017/. Publisher: Copernicus GmbH.

de Vos, L.W., Leijnse, H., Overeem, A., Uijlenhoet, R., 2019. Quality control for crowdsourced personal weather stations to enable operational rainfall monitoring. Geophys. Res. Lett. 46, 8820–8829. https://doi.org/10.1029/2019GL083731. URL https://agupubs.onlinelibrary.wiley.com/doi/abs/10.1029/2019GL083731. _eprint: https://agupubs.onlinelibrary.wiley.com/doi/pdf/10.1029/2019GL083731.

Winterrath, T., Brendel, C., Hafer, M., Junghänel, T., Klameth, A., Lengfeld, K., Walawender, E., Weigl, E., Becker, A., 2018. Radar Climatology (Radklim) Version 2017.002: Reprocessed Quasi Gauge-Adjusted Radar Data, 5-Minute Precipitation Sums (YW). https://doi.org/10.5676/DWD/RADKLIM_YW_V2017.002.

Winterrath, T., Rosenow, W., Weigl, E., 2012. On the DWD quantitative precipitation analysis and nowcasting system for real-time application in German flood risk management. IAHS Publ. 351, 7.

Zheng, F., Tao, R., Maier, H.R., See, L., Savic, D., Zhang, T., Chen, Q., Assumpção, T.H., Yang, P., Heidari, B., Rieckermann, J., Minsker, B., Bi, W., Cai, X., Solomatine, D., Popescu, I., 2018. Crowdsourcing methods for data collection in geophysics: state of the art, issues, and future directions. Rev. Geophys. 56, 698–740. https://doi.org/10.1029/2018RG000616. URL https://agupubs.onlinelibrary.wiley.com/doi/abs/10.1029/2018RG000616. _eprint: https://agupubs.onlinelibrary.wiley.com/doi/pdf/10.1029/2018RG000616.